Solvent Dependence of the Spectra and Kinetics of Excited-State Charge Transfer in Three (Alkylamino)benzonitriles

K. Dahl,[†] R. Biswas,[‡] N. Ito, and M. Maroncelli*

Department of Chemistry, Penn State University, University Park, Pennsylvania 16802

Received: July 29, 2004; In Final Form: November 10, 2004

Steady-state absorption and emission spectra and emission decay kinetics are reported for 4-aminobenzonitrile (ABN), 4-(1-azetidinyl)benzonitrile (P4C), 4-(1-pyrrolidinyl)benzonitrile (P5C), and 4-(1-piperidinyl)-benzonitrile (P6C) in 24 room temperature solvents. In solvents of modest to high polarity, P4C, P5C, and P6C exhibit dual fluorescence and emission decays characteristic of the transformation from an initially prepared (LE) state to a more polar charge transfer (CT) state, whereas ABN does not undergo this reaction. The frequencies of the steady-state absorption and emission spectra of all of these solutes can be rationalized using a dielectric continuum description of the solvent and considering only the minima on the reactive surfaces, which are assumed to involve both an intramolecular (twisting) and a solvation coordinate. Characteristics of the gas-phase solutes deduced from this analysis are in good agreement with electronic structure calculations and indicate that differences in their spectra mainly reflect differences in the relative energies of the gas-phase LE and CT states. The relative yields of LE and CT emission are not described as satisfactorily by this model, and reasons for this failure are discussed. The kinetics of the LE → CT reaction vary considerably with solute and solvent. In many solvents, the emission decays of P4C are reasonably described by a simple two-state kinetic scheme with time-independent rate constants. In P5C and P6C multiexponential decays are observed that reflect time-dependent shifts of the component spectra as well as time-dependent reaction rates. A simplified analysis of these complex dynamics provides estimates for both the free energy change $\Delta_r G$ and (average) LE → CT rate constant k_f for a wide range of solute and solvent combinations. The driving force for reaction ($-\Delta_r G$) follows the order P6C > P5C > P4C and increases with increasing solvent polarity. The reaction rates are correlated to $\Delta_r G$ and follow the opposite trend. The relationships observed between k_f and $\Delta_r G$ suggest that static solvent effects, i.e., barrier height changes, are the primary determinants of the solvent dependence in P4C. Correlations between barrier-corrected rates and solvation times suggest that dynamical solvent effects contribute substantially to the solvent dependence of the rates in P5C, and especially P6C.

I. Introduction

The excited-state reaction leading to the dual fluorescence of 4-dimethylaminobenzonitrile (DMABN; Scheme 1) and related compounds has been actively studied since its initial discovery in the early 1960s.[1−3] A number of models have been advanced to explain the nature of the "anomalous" red-shifted fluorescence that occurs in addition to the "normal" fluorescence of DMABN and its analogues in polar environments. The history of these various models and a discussion of the evidence for each is contained in the recent comprehensive review by Grabowski et al.[1] All models attribute the polarity-sensitive anomalous fluorescence to an electronic state of charge transfer (CT) character. The state emitting normal fluorescence is supposed to be of "locally excited" (LE) character, i.e., one possessing a charge distribution similar to that of the ground state. Relative to this state, the CT state is envisioned to involve transfer of substantial charge from the amino group to the benzonitrile ring. In addition, some type of intramolecular rearrangement is generally assumed to accompany charge transfer, but the various models disagree about the specifics of this rearrangement. Much experimental and theoretical evidence supports one of the earliest models, the "twisted intramolecular charge transfer" (TICT) mechanism, illustrated in Scheme 1. In this model, charge transfer occurs in concert with a twisting of the alkyl group from a conformation roughly coplanar with the benzonitrile ring to a perpendicular arrangement. Despite many years of scrutiny and debate,[1] the correctness of this model is not universally accepted. There are several pieces of experimental evidence, such as the presence of CT emission in planarized aminobenzonitriles,[4,5] that are difficult to reconcile with the TICT model, and have led some researchers to favor other hypotheses.[6,7] For modeling purposes, we assume the basic correctness of the TICT idea, at least in the case of unhindered amino derivatives, but recognize that other intramolecular changes may also accompany the LE → CT conversion.

SCHEME 1

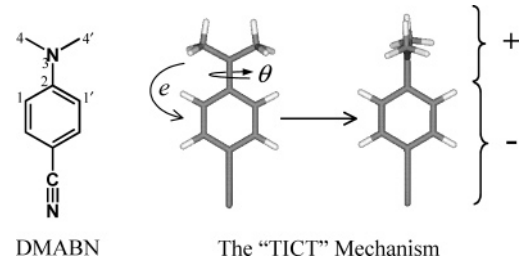

DMABN The "TICT" Mechanism

[†] Current address: U.S. Naval Research Laboratory, Washington, D.C.
[‡] Current address: S. N. Bose National Center for Basic Sciences, Salt Lake, Kolkata, India.

10.1021/jp046605p CCC: $30.25
Published on Web 01/05/2005

SCHEME 2

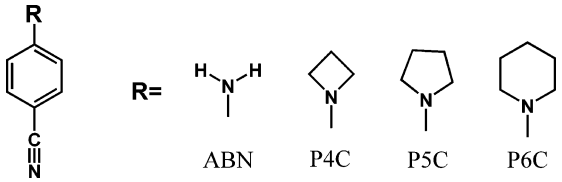

In the present work we examine the excited-state reactions of the three dialkylaminobenzonitrile molecules depicted in Scheme 2. These molecules are similar in most respects to DMABN and, although less extensively investigated, offer advantages for our purposes. The five- and six-membered ring compounds were introduced as DMABN analogues by Rettig in 1980[8] and studied in a number of contexts by Rettig's group and their collaborators.[9−18] Zachariasse and co-workers examined all of the compounds with ring sizes between 3 and 8 atoms,[19−21] dubbing them the "P*n*C" series (n = number of ring atoms), a notation we adopt here. In addition to these experimental studies, semiempirical,[22,23] density functional,[24] and ab initio[23] calculations have been performed on the P*n*C series.

The collective outcome of this work may be summarized as follows. In the ground state, P3C−P5C have energy minima in untwisted ($\theta \sim 0°$) geometries. For steric reasons, P6C, on the other hand, is twisted by ~30.[8,10,13] The amino groups are generally nonplanar, exhibiting some degree of pyramidalization, with the pyramidalization angle increasing substantially in the smaller rings.[22−24] In the S_1 state, these molecules generally adopt a more nearly planar conformation about the amino group. Two electronic states, an ^1L_b state and a more polar ^1L_a state, make up the S_1 surface on which the LE → CT reaction occurs. Both in the gas phase and in solution the L_b state lies lowest in energy for untwisted geometries, whereas the L_a state is generally lower near $\theta = 90°$. The LE → CT transition therefore involves a change in character of the S_1 state from an LE state of L_b character to a CT state of L_a character as the molecule twists. In the gas phase, the energy of the S_1 state is a maximum at the 90° twisted conformation and the CT state is unobservable. However, the large dipole moment of the ^1L_a state and the fact that it increases significantly with twist angle enables the twisted conformation (i.e., the TICT state) to become a minimum on the S_1 surface in sufficiently polar solvents. The variations in behavior of the members of the P*n*C series can be traced mainly to the systematic decrease in N pyramidalization with ring size, which decreases the energy of the L_a state relative to the L_b state. This energy modulation is such that for the smallest member of the series, P3C, the CT state never becomes an energy minimum, even in highly polar solvents, and only LE emission is observed.[19] The remaining members of the series do show CT emission in a highly polar solvent like acetonitrile, and the relative amount of CT versus LE emission increases in the order P4C < P5C ~ DMABN < P6C. This variation, in large part at least, reflects the variation in the relative energies of the solvated CT and LE states resulting from these changes in ring energetics. It should also be noted that P6C differs from DMABN and the other members of the series studied here in having a nonzero twist angle in both the ground and LE states.

There have been a number of prior studies of the kinetics of the LE → CT reaction in some members of the P*n*C series. Several measurements show that the reaction rates tend to follow the same trend as the steady-state intensity ratios, i.e., P4C < P5C ~ DMABN < P6C.[9,19,21] Zachariasse and co-workers[19] measured the time-resolved emission of P4C and P5C in acetonitrile over the temperature range 230−300 K, using an instrument with a response time of 30−40 ps. The observed emission decays could be described by a two-state kinetic scheme and interpreted in terms of conventional activated kinetics. They concluded that the reaction in P4C is ~20 times slower than in P5C at room temperature as a result of a roughly 2-fold larger barrier to reaction. Rettig and co-workers also reported several measurements of time-resolved emission (~600 ps instrument response) in low-temperature solvents.[9,14,16,17] In one study, they measured the LE decays of P5C and P6C in six solvents and solvent mixtures near 200 K. At such temperatures the LE → CT reaction is irreversible and the LE emission is expected to decay exponentially if the reaction is a simple activated process. In the more polar solvents examined, Rettig and co-workers found markedly nonexponential kinetics in both P5C and P6C,[14] reminiscent of what has been observed for DMABN in alcohol solvents.[25−28] Similar complex kinetics were observed for both P5C and DMABN in the high-viscosity solvents glycerol and triacetin.[16] They found that at high viscosities the rates of the two reactions are approximately equal and depend only on solvent viscosity (altered either by temperature or pressure variations). Rettig and co-workers interpreted their observations to mean that the LE → CT reaction is a barrierless process controlled by solvent friction. Support for this idea was found in the dependence of the CT/LE intensity ratio and the early decay kinetics observed in 1-propanol at low temperature.[17]

Our interest in the P*n*C molecules is to use them to further explore the relationship between polar solvation dynamics[29−31] and charge transfer.[32] At room temperature, the available data[19,21] suggest that the LE → CT interconversion ranges from being much slower than polar solvation times of most solvents[33,34] in the case of P4C, to being faster or comparable to solvation times in the case of P6C. This situation, coupled to the information on the energetics of reaction available from their steady-state spectroscopy, renders the P*n*C series an excellent choice for such investigations. An interesting aspect of this work will be to sort out the roles played by solvent friction on the charge transfer, i.e., the "dielectric" part of the friction, which is most closely related to the dynamics of polar solvation, and the "mechanical" or viscous friction operating on the large-amplitude twisting motion. We believe that the best way to deal with this dual effect of solvent friction is to view these reactions as taking place on two-dimensional free energy surfaces in which one coordinate describes the solvation state and the other the intramolecular twisting coordinate. This perspective has already been employed in the context of analytical theories of electron transfer[35,36] to model the DMABN reaction in alcohol solvents[28,37] and in more realistic model potentials by several groups.[38−47] What distinguishes our efforts from those of earlier workers is that before modeling the reaction dynamics, we seek to develop 2-dimensional solution-phase potentials that can accurately reproduce the steady-state absorption and emission spectra of these molecules in a variety of solvents. Such potentials can then be used together with what is known about polar solvation dynamics to confidently sort out the roles played by dielectric and mechanical friction in these reactions.

The present paper documents our initial steps toward developing such solution-phase potentials. Herein, we report the characterization of the steady-state spectra of P4C, P5C, and P6C, together with the nonreactive analogue ABN, in 24 room-temperature solvents. Rather than attempting a complete analysis in terms of 2-dimensional potentials, we examine a simplified model that focuses only on isolated points on these potentials and ignores the effects of distributions over coordinates. We

find that such a simplified model, using a dielectric continuum representation of solvation, is sufficient to represent the observed spectral frequencies to reasonable accuracy. Moreover, the characteristics of the solutes derived from this analysis are in good accord with predictions of electronic structure calculations. However, the solvent dependence of the relative intensities of the LE and CT emission cannot be reproduced with this model, presumably as a result of the importance of the distribution of twist angles in determining the nominally forbidden CT emission intensity. We also survey the kinetics of the excited-state reactions of P4C, P5C, and P6C in all of these solvents at room temperature. In some cases, such as P4C in most solvents, the emission decays are well described by a simple two-state scheme with time-independent rate constants. In many other solute + solvent combinations the emission is more complex, reflecting both continuous spectral relaxation and time-dependent reaction rates, which we ascribe to the small ($<10\ k_BT$) barriers to reaction in most of the systems examined. Correlations between the rates and driving force for reaction indicate that dynamical solvent effects play an important role in determining reaction rates in P5C and P6C, and little or no role in the case of P4C. These differences appear to reflect mainly the solute dependence of the barrier heights set by the different gas-phase energies of the LE and CT states in these three solutes.

The remainder of this work is structured as follows. Section II details the experimental and computational procedures used, and section III reviews the two-state kinetic scheme employed in modeling. The solvent dependence of the steady-state spectra are described in section IV, and measurements of quantum yields, radiative rates, and transition moments in several solvents are then presented in section V. The theoretical model used to describe the 2-dimensional solution-phase potentials and fits of the data to a simplified version of this model are describe in section VI. Electronic structure calculations are used to guide the modeling and some results of ab initio and semiempirical calculations on the P*n*C series are also presented in this section. Finally, kinetic data are presented and interpreted in a semi-quantitative fashion in section VII.

II. Experimental and Computational Methods

4-Aminobenzonitrile (ABN) was purchased from Aldrich and recrystallized three times from cyclohexane. 4-(1-Azetidinyl)-benzonitrile (P4C), 4-(1-pyrrolidinyl)benzonitrile (P5C), and 4-(1-piperidinyl)benzonitrile (P6C) were synthesized following literature procedures,[8] recrystallized three times from cyclohexane, and sublimed. Purity was verified by TLC and HPLC, and proved to be better than 99.5% in all cases. Solvents were typically spectrophotometric grade (99+%) from Aldrich. The "perfluorohexanes" solvent was a mixture of hexane isomers of 98% purity from Lancaster Synthesis. Solvents were used as received, with one exception, tetrahydrofuran (THF). Using THF as received produced inconsistent spectra of P5C, which showed variable LE/CT intensity ratios as well as substantial excitation wavelength dependence, presumably due to the presence of acidic impurities. Passing the THF through a column containing activated basic alumina eliminated these problems, and resulted in consistent behavior between different samples. Treatment of other low-polarity solvents in this manner had no effects on the steady-state emission.

Samples for steady-state spectroscopy were prepared in 1 cm quartz cuvettes at concentrations providing optical densities of less than 0.1. Absorption measurements were made using a Hitachi U-3000 UV/vis spectrophotometer with a resolution of 1 nm. Corrected emission and excitation spectra were recorded with a Spex Fluorolog F212 spectrometer at 2 nm resolution. Solvent blanks were subtracted from the emission spectra prior to analysis. Initial experiments with and without N_2 bubbling showed that atmospheric oxygen had little effect on the spectra or dynamics of interest here, and most samples were therefore not deoxygenated. (Oxygen quenching does shorten the overall emission lifetimes of these compounds slightly, but we make no use of these times in the present work.) For analysis, emission spectra were converted to a frequency representation using the requisite λ^2 reweighting of intensities. Emission quantum yields φ were measured relative to the standard quinine sulfate dihydrate in 0.05 M H_2SO_4, whose quantum yield was taken to be $\varphi_R = 0.508$,[48] using the relation

$$\varphi_S = \varphi_R \left(\frac{n_R^2}{n_S^2}\right)\left(\frac{I_S}{I_R}\right)\left(\frac{1 - 10^{-0.5A_R}}{1 - 10^{-0.5A_S}}\right) \qquad (2.1)$$

where n is the solvent refractive index, I the integrated emission intensity, and A the absorbance of the sample (S) and reference (R) solutions. The accuracy of the quantum yields reported here is expected to be better than ±10%. The quantum yield measurements were performed at 25.0 ± 0.2 °C using a circulating water bath. Other steady-state spectra were recorded at room temperature, 23 ± 2 °C.

Time-resolved emission data were collected using a time-correlated single-photon instrument based on a fs Ti:sapphire laser.[49] Samples were contained in 1 cm cuvettes into which filter glass was inserted to remove reflections near time zero. The samples were maintained at 25.0 ± 0.2 °C using a circulating water thermostat. Emission was collected at magic angle through an ISA H10 monochromator with an emission band-pass of 8 nm. The response time of this instrument was ~25 ps (fwhm). Data were collected with variable resolution (1−6 ps/channel) and over variable time windows (2−12 ns) to best capture the decay kinetics. In most cases, two or three pairs of LE and CT decays were collected for each solute + solvent combination and the average over these data sets are reported. Decays at either a single wavelength or at multiple wavelengths were fit to multiexponential forms using an iterative reconvolution algorithm. Such fitting allows decay components as fast as ~5 ps to be measured with reasonable accuracy. Time-resolved emission spectra were reconstructed from a series of 10−20 emission decays using the steady-state spectrum for relative normalization as described in ref 33.

Electronic structure calculations were performed at two levels. Ground-state properties were calculated at the MP2/6-31G(d)//RHF/6-31G(d,p) level of theory using the Gaussian98 program.[50] Excited-state properties were calculated at the AM1/CI level using the program AMPAC 6.55.[51] The latter calculations involved ~100 energy-selected configurations on the complete active space generated from the five orbitals surrounding the HOMO−LUMO gap. Some AM1/CI calculations included the effect of a dielectric continuum solvent using the COSMO[52] self-consistent reaction field approach.[53,54] This method uses a realistic cavity shape generated by the van der Waals surface of the solute extended by some spherical solvent size. The latter parameter was chosen to be 2.6 Å in the present work to achieve reasonable agreement with the observed solvent dependence of transition energies. This value is close to the radius corresponding to the average van der Waals volume of the set of solvents examined here, 2.7Å. Twist angles are defined as the average torsional angle made by atoms 1, 2, 3, 4 and 1′, 2, 3, 4′ shown in Scheme 1.

SCHEME 3

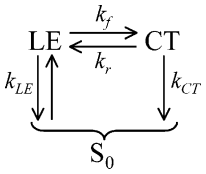

III. Kinetic Framework and Nomenclature

In all cases studied the time-dependent emission of the P*n*C solutes appears to reflect a two-state LE ⇀ CT interconversion process. In many cases, the observed emission decays conform to what is expected on the basis of the conventional reversible reaction with time-independent rate constants depicted in Scheme 3. Although there are also many solute + solvent combinations that display more complicated behavior, this simple model provides a useful starting point for describing our observations. We therefore outline the key implications of such a scheme and introduce the notation to be used throughout the remainder of this work.

The excited-state accessed by photon absorption from S_0 is designated the "LE" ("locally excited") state and the product of the excited-state reaction the "CT" ("charge transfer") state. These two states decay to the ground state with net (radiative plus nonradiative) rate constants k_{LE} and k_{CT} and interconvert according to the forward and reverse rate constants k_f and k_r. All rate constants are here assumed to be time-independent. Under the assumption of no CT excitation, the populations of the LE and CT states at a time t after excitation, [Z(t)], and their respective emission intensities, $I_Z(t)$, are given by the well-known relations[55]

$$I_{LE}(t) \propto k_{LE}^{rad}\frac{[LE(t)]}{[LE(0)]} = k_{LE}^{rad}\frac{1}{\lambda_+ - \lambda_-}\{(Y-\lambda_-)e^{-\lambda_- t} + (\lambda_+ - Y)e^{-\lambda_+ t}\}$$

$$I_{CT}(t) \propto k_{CT}^{rad}\frac{[CT(t)]}{[LE(0)]} = k_{CT}^{rad}\frac{k_f}{\lambda_+ - \lambda_-}\{e^{-\lambda_- t} - e^{-\lambda_+ t}\} \quad (3.1)$$

where

$$\lambda_\pm = \frac{1}{2}\{(X+Y) \pm \sqrt{(X-Y)^2 + 4k_f k_r}\}$$
$$X = k_{LE} + k_f \quad \text{and} \quad Y = k_{CT} + k_r \quad (3.2)$$

and where k_Z^{rad} is the radiative rate constant of state Z. Integration of eq 3.1 provides the quantum yields for LE and CT emission,

$$\varphi_{LE} = k_{LE}^{rad}\left[\frac{Y}{\lambda_+\lambda_-}\right] = k_{LE}^{rad}\left[\frac{k_{CT}+k_r}{(k_{LE}k_{CT} + k_{LE}k_r + k_{CT}k_f)}\right]$$
$$\varphi_{CT} = k_{CT}^{rad}\left[\frac{k_f}{\lambda_+\lambda_-}\right] = k_{CT}^{rad}\left[\frac{k_f}{(k_{LE}k_{CT} + k_{LE}k_r + k_{CT}k_f)}\right] \quad (3.3)$$

and their ratio:

$$\frac{\varphi_{CT}}{\varphi_{LE}} = \left(\frac{k_{CT}^{rad}}{k_{LE}^{rad}}\right)\left(\frac{k_f}{k_{CT}+k_r}\right) \quad (3.4)$$

Near to room temperature, the excited-state reactions of the P*n*C solutes are generally rapid compared to the LE and CT decay rates (see section VII). If one therefore assumes that k_f, $k_r \gg k_{LE}$, k_{CT} the above equations simplify to

$$I_{LE}(t) \propto k_{LE}^{rad}\frac{1}{1+K_{eq}}\{e^{-k_{dec}t} + K_{eq}e^{-k_{rxn}t}\}$$

$$I_{CT}(t) \propto k_{CT}^{rad}\frac{K_{eq}}{1+K_{eq}}\{e^{-k_{dec}t} - e^{-k_{rxn}t}\} \quad (3.5)$$

where $K_{eq} = k_f/k_r$ is the equilibrium constant for the reaction,

$$k_{rxn} = k_f + k_r \quad (3.6)$$

is the rate constant associated with reactive equilibration, and

$$k_{dec} = {}^1/_2(k_{LE} + k_{CT}) \quad (3.7)$$

is the average excited-state population decay constant. The quantum yields become

$$\varphi_{LE} = \frac{k_{LE}^{rad}}{k_{dec}}\left(\frac{1}{1+K_{eq}}\right) \qquad \varphi_{CT} = \frac{k_{CT}^{rad}}{k_{dec}}\left(\frac{K_{eq}}{1+K_{eq}}\right)$$
$$\frac{\varphi_{CT}}{\varphi_{LE}} = \left(\frac{k_{CT}^{rad}}{k_{LE}^{rad}}\right)K_{eq} \quad (3.8)$$

Thus, in this limit, the ratios of band areas in the steady-state spectra reflect the equilibrium constant for the excited-state reaction to within a factor of the radiative rates of the two states. This limit is assumed in deriving transition moments in section V, in fitting the relative CT/LE band ratios in the steady-state spectra in section VI, and in deriving K_{eq} and k_f from decay times and amplitudes in section VII.

The emission decays derived from Scheme 3 are biexponential functions of time when viewed anywhere in the spectrum. In some cases the decays observed in the LE region are more complex than biexponential functions and can only be accurately fit to sums of three or more exponential components. As discussed in section VII, this more complicated behavior appears to be related to the breakdown of the assumption of time-independent rate constants as a result of the small barriers to reaction in many of the systems studied here. In such cases it is not generally possible to derive analytic expressions comparable to those described above. Nevertheless, if one makes the reasonable assumption that only the forward reaction involves a time-dependent rate constant, a simple relationship must exist between the concentrations of LE and CT molecules if the reaction involves only these two species.[25] Assuming that the populations behave according to the differential relations,

$$\frac{d[LE]}{dt} = -k_{LE}[LE] - k_f(t)[LE] + k_r[CT] \quad (3.9a)$$

$$\frac{d[CT]}{dt} = -k_{CT}[CT] - k_r[CT] + k_f(t)[LE] \quad (3.9b)$$

if [LE(t)] is known, [CT(t)] can be obtained by solving the differential equation

$$\frac{d[CT]}{dt} = -k_B[CT] - \frac{d[LE]}{dt} + k_{LE}[LE] \quad (3.10)$$

Assuming that [LE(t)] is characterized using a multiexponential form

$$[LE(t)] = \sum_i a_i \exp(-r_i t) \quad (3.11)$$

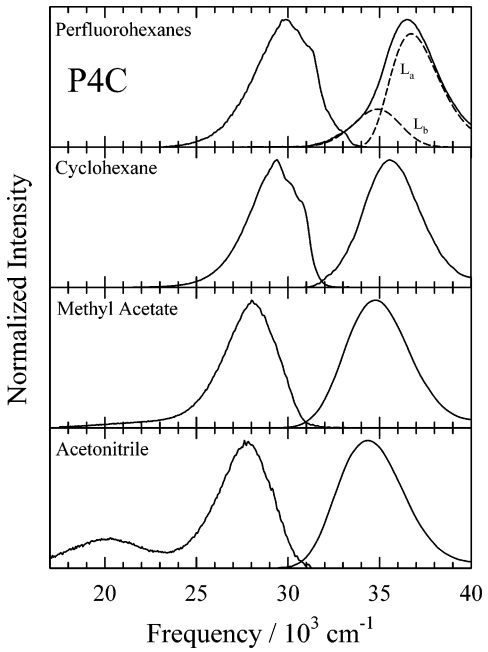

Figure 1. Absorption and emission spectra of P4C in four solvents of varying polarity (dielectric constants in parentheses): perfluorohexanes (1.6), cyclohexane (2.0), methyl acetate (6.7), and acetonitrile (35.9). The absorption spectrum in perfluorohexanes has been schematically decomposed into contributions from underlying ^1L_a and ^1L_b absorption bands, based on an assumed shape for the ^1L_a band.

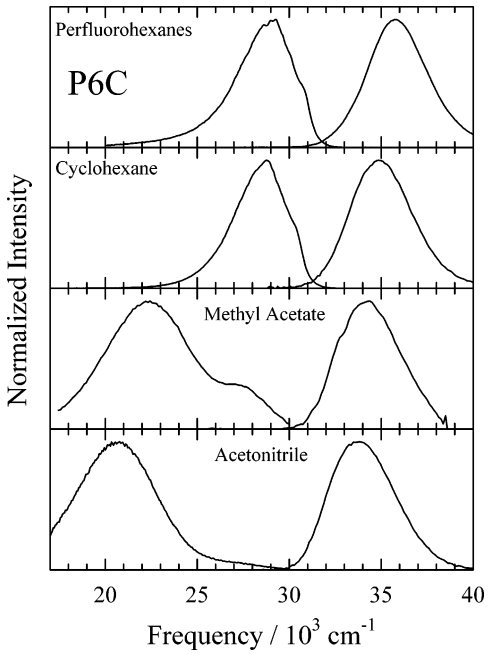

Figure 2. Absorption and emission spectra of P6C in four solvents of varying polarity.

eq 3.10 can be solved explicitly for [CT(t)]:

$$[\mathrm{CT}(t)] = \sum_i \left(\frac{r_i - k_{\mathrm{LE}}}{r_i - k_{\mathrm{CT}}}\right) a_i \{\exp(-k_{\mathrm{CT}}t) - \exp(-r_i t)\}$$

$$= (\sum_i b_i) \exp(-k_{\mathrm{CT}}t) + \sum_i (-b_i) \exp(-r_i t)$$

$$b_i = \frac{r_i - k_{\mathrm{LE}}}{r_i - k_{\mathrm{CT}}} \qquad (3.12)$$

Equations 3.11 and 3.12 will be used in section VII to verify the precursor−successor relationship between the LE and CT states in cases where emission decays are not biexponential.

IV. Steady-State Spectra

Figures 1 and 2 display representative absorption and emission spectra of the P4C and P6C in four solvents of varying polarity. Corresponding spectra of ABN and P5C are provided in the Supporting Information. All of these spectra are similar to ones previously reported by Zachariasse and co-workers.[19−21] The absorption spectra in nonpolar solvents suggest the presence of more than one low-lying electronic transition. In addition to the main absorption band assigned to the $S_0 \rightarrow {}^1L_a$ transition, a "foot" on the low-frequency edge of the spectra in nonpolar solvents signals the presence of the weaker $S_0 \rightarrow {}^1L_b$ transition.[1] A schematic decomposition is shown in the upper panel of Figure 1. In polar solvents, the stronger ^1L_a band shifts to lower frequencies and broadens, masking the presence of overlapping transitions. The emission of all three compounds consists of a single structured band in nonpolar solvents, which we designate as the LE emission. This LE band is the only emission detected for the control compound ABN. In sufficiently polar solvents, P4C, P5C, and P6C show, in addition to the LE band, the "anomalous" red-shifted emission band characteristic of DMABN analogues. We designate this latter band the "CT" emission. Comparison of the spectra of the three P*n*C solutes in the same polar solvent shows that the CT/LE emission intensity ratio increases in the order P4C < P5C < P6C. As we will show later, this trend reflects the relative lowering of the CT energy relative to the LE energy as one progresses to larger alkyl rings within this series of solutes.

Characteristics of the absorption and emission spectra of ABN and the P*n*C solutes were determined in 24 solvents. Table 1 lists these solvents and illustrates the sort of data collected for the case of P5C. Corresponding summaries for the remaining solutes are contained in Tables S1−S3 of the Supporting Information. The arrangement of solvents here is such that polar aprotics are listed first, followed by normal alcohols and other protic solvents. Within each grouping, solvents are approximately ordered in terms of increasing polarity. The frequencies ν_{abs} and bandwidths Γ_{abs} are the peak positions and full-width at half-maximum (fwhm) of the entire absorption band. It was not possible to decompose the absorption spectra into separate ^1L_a and ^1L_b contributions, but we believe that the peak frequencies reported here should be a reasonable representation of the solvent dependence of the $S_0 \rightarrow {}^1L_a$ transition.

To analyze emission spectra of a given solute, we used as a reference its spectrum in perfluorohexanes, the least interactive solvent. Spectra in other solvents were least-squares fit to a model consisting of one or two emission bands derived from shifted and broadened versions of this reference spectrum. Examples of such fits are illustrated in Figure 3. As shown here, convolution of the spectrum in perfluorohexanes with a Gaussian function (representing inhomogeneous solvent broadening) provides a good representation of the observed LE band shapes. The broader CT emission band is also well represented in this manner. The LE and CT frequencies, bandwidths, and area ratios listed in Table 1 and used in subsequent analysis are all derived from such fits.

The spectra of all of the solutes studied here share a number of similarities. First, beyond the differences in quantum yield (section V) in none of the solutes is there a clear distinction between spectra in protic versus aprotic solvents. Thus, specific hydrogen bonding does not appear to affect the spectral shifts, line widths, or CT/LE ratios. Although there is some variability in the structure exhibited in some bands in nonpolar solvents,

TABLE 1: Characteristics of the Steady-State Spectra of P5C[a]

solvent	$d_{0.25}(\epsilon)$	ν_{abs}	Γ_{abs}	ν_{LE}	Γ_{LE}	ν_{CT}	Γ_{CT}	$\varphi_{CT}/\varphi_{LE}$
perfluorohexanes	.15	36.02	3.06	30.05	3.56			
n-hexane	.20	35.33	3.36	29.66	3.49			
methylcyclohexane	.23	35.15	3.63	29.60	3.45			
cyclohexane	.23	35.21	3.46	29.60	3.53			
benzene	(0.2)	33.96	3.82	28.60	3.56	23.55*	3.48*	0.05 ± 0.03
diethyl ether	0.41	34.89	3.77	28.83	3.58	23.55*	4.32*	0.09 ± 0.05
dichloromethane	0.53	33.52	4.05	28.30	3.63	22.15	4.82	1.5 ± 0.8
1,4-dioxane	(0.2)	34.36	3.99	28.43	3.62	22.64*	4.95*	0.3 ± 0.2
tetrahydrofuran	0.51	34.31	4.02	28.29	3.62	22.02	5.05	0.75 ± 0.11
ethyl acetate	0.48	34.41	3.95	28.28	3.65	21.76	5.08	1.0 ± 0.1
methyl acetate	0.49	34.36	3.96	28.21	3.66	21.51	5.08	1.4 ± 0.2
dimethylformamide	0.63	33.45	4.07	27.59	3.71	19.71	5.00	7 ± 2
dimethyl sulfoxide	0.64	33.10	4.08	27.52	3.93	19.20	5.08	6 ± 1
acetonitrile	0.63	33.87	4.15	27.71	3.95	20.00	4.92	7 ± 2
methanol	0.63	33.77	4.29	28.19	3.95	19.45	5.25	6 ± 1
ethanol	0.61	33.77	4.23	28.34	3.85	19.93	5.33	6 ± 1
1-propanol	0.60	33.73	4.27	28.43	3.76	20.20	5.35	5.1 ± 1.1
2-propanol	0.60	33.81	4.18	28.41	3.78	20.37	5.36	4.6 ± 1.0
1-butanol	0.59	33.68	4.25	28.49	3.77	20.39	5.38	4.2 ± 0.9
1-pentanol	0.58	33.78	4.26	28.50	3.63	20.56	5.39	3.7 ± 0.8
1-decanol	0.52	34.04	4.32	28.74	3.62	21.83	5.31	1.0 ± 0.1
N-methylformamide	0.66	33.29	4.13	27.52	3.64	19.23	5.22	8 ± 4
ethylene glycol	0.63	32.95	4.27	28.06	3.82	18.90	5.38	2.9 ± 0.8
formamide	0.65	32.76	4.10	27.80	3.66	18.79	5.19	5.1 ± 1.1

[a] $d_{0.25}(\epsilon)$ are values of the reaction field factor defined by eq 4.1. They are provided here as measures of solvent "polarity". Peak frequencies (ν) and bandwidths (Γ, fwhm) are in units of 10^3 cm^{-1}. $\varphi_{CT}/\varphi_{LE}$ are the ratios of the areas of the CT and LE emission bands. Data were recorded at room temperature, 23 ± 2 °C. Estimated uncertainties in the frequencies and widths are ± 300 cm^{-1} in absorption (uncertainty in L_a position) and ± 170 cm^{-1} in emission unless noted otherwise. Uncertainties of the CT data marked with asterisks are ± 300 cm^{-1}.

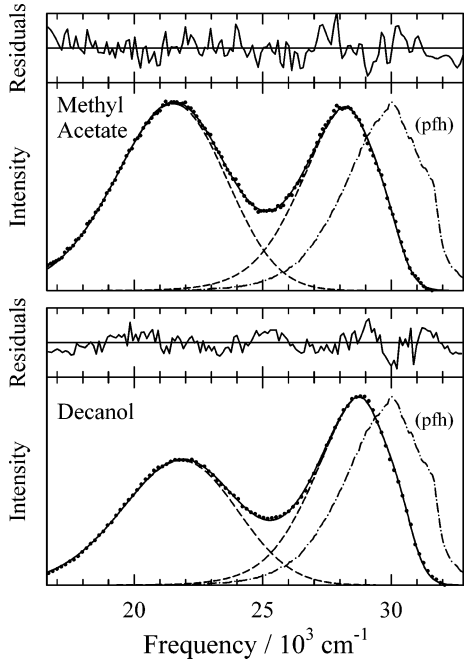

Figure 3. Representative fits to emission spectra of P5C. Experimental spectra are shown as points (thinned for clarity), the overall fit as a solid line, and the LE and CT contributions as dashed lines. The perfluorohexanes spectrum used as a reference line shape for fitting is shown by the dash−dot curve labeled "pfh". The residuals are shown on a scale that is ±3% of the scale on which spectra are displayed.

the widths of the respective spectra are nearly equal in all of the solutes, as illustrated by the average values provided in Table 2. The values of $\langle\Gamma\rangle$ listed here are the full widths of the respective bands averaged over all of the solvents studied. The widths do vary with solvent, increasing with the magnitude of the solvent-induced frequency shift, as would be expected. This dependence is roughly quantified in the last columns of Table 2, which list the slopes observed upon correlating the widths and frequencies of the observed spectra ($d\Gamma/d\nu$) and the inhomogeneous broadening and shift relative to the reference spectra in perfluorohexanes ($d\gamma/d\delta$). To within the large uncertainties in these derivative quantities, the solvent dependence of the various bandwidths are also similar in all four solutes. A curious feature of these data is that the width of the CT band is much less sensitive to frequency shift (solvent polarity) than are the LE and absorption bands. This behavior is contrary to the expectation that the solvent-induced broadening and shift (reorganization energy) of the spectra should be simply related.[56] The weaker-than-expected solvent dependence of the CT bandwidth was noted as a feature common to DMABN and other derivatives,[1] and it represents an important puzzle in understanding their spectroscopy.

One primary interest in this work is the solvent dependence of the frequencies of the various bands and CT/LE intensity ratios. We will attempt to interpret this solvent dependence in terms of an overall model of the excited-state reaction in section VI. To provide a less model-dependent characterization of these quantities, here we examine how they correlate to dielectric reaction field factors of the sort

$$d_c(\epsilon) = \frac{\epsilon - 1}{2(1 - c)\epsilon + (1 + 2c)} \qquad (4.1)$$

where ϵ is the solvent dielectric constants and c is a solvent-independent parameter $0 \le c \le 1$. (Dielectric constants and other properties of the solvents used here are provided in Table S4.) This functional form will be motivated in section VI. Here we only note that different values of c reflect different possible choices for the solute polarizability. Values of $c = 0$ and $c = 0.5$ yield the two most popular reaction field functions,[57,58] $d_0(\epsilon) = (\epsilon - 1)/(2\epsilon + 1)$ (nonpolarizable solute) and $d_{0.5}(\epsilon) = (\epsilon - 1)/(\epsilon + 2)$. Whereas any value of c in this range correlates the experimental data equally well, for reasons to be described later, we prefer an intermediate value $c = 0.25$. Correlations between the spectral data and $d_{0.25}(\epsilon)$ are shown in Figures 4

TABLE 2: Bandwidths and Their Relation to Frequency[a]

species	$\langle\Gamma_{abs}\rangle/10^3$ cm^{-1}	$\langle\Gamma_{LE}\rangle/10^3$ cm^{-1}	$\langle\Gamma_{CT}\rangle/10^3$ cm^{-1}	$-(d\Gamma/d\nu)_{abs}$	$-(d\gamma/d\delta)_{LE}$	$-(d\gamma/d\delta)_{CT}$
ABN	4.0	3.6		0.48 ± 0.07	0.59 ± 0.09	
P4C	4.2	3.7	5.1	0.41 ± 0.04	0.48 ± 0.07	0.23 ± 0.19
P5C	4.0	3.7	5.2	0.34 ± 0.05	0.69 ± 0.14	0.09 ± 0.05
P6C	4.1	3.6	5.2	0.35 ± 0.09	0.52 ± 0.13	0.21 ± 0.07

[a] $\langle\Gamma_x\rangle$ denotes the average width (fwhm) of the observed band x. γ denotes the width (fwhm) and δ the average frequency of the Gaussian function that, when convoluted with the reference line shape, best matches the observed band. Average widths are averages over all solvents where reliable data were available. Derivative quantities are the slopes of the least-squares linear relations between Γ and ν or between γ and δ.

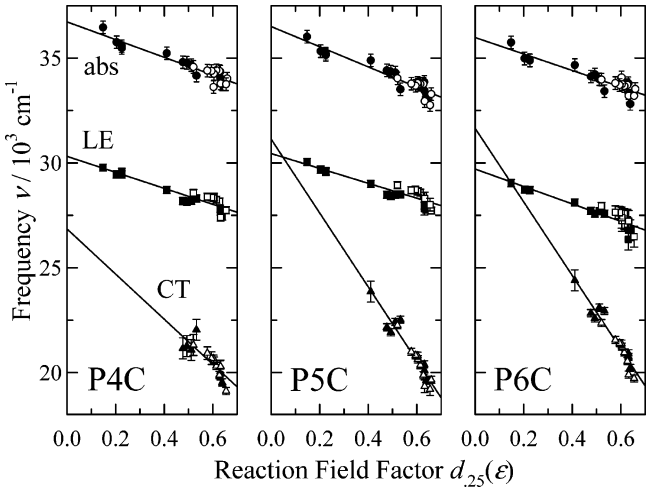

Figure 4. Absorption, LE, and CT emission frequencies of P4C, P5C, and P6C plotted against the reaction field factor $d_c(\epsilon)$ ($c = 0.25$). Filled and open symbols denote aprotic and protic solvents, respectively. Data in benzene and dioxane are excluded from these figures. The lines are the least-squares fits, whose parameters are provided in Table S4 of the Supporting Information.

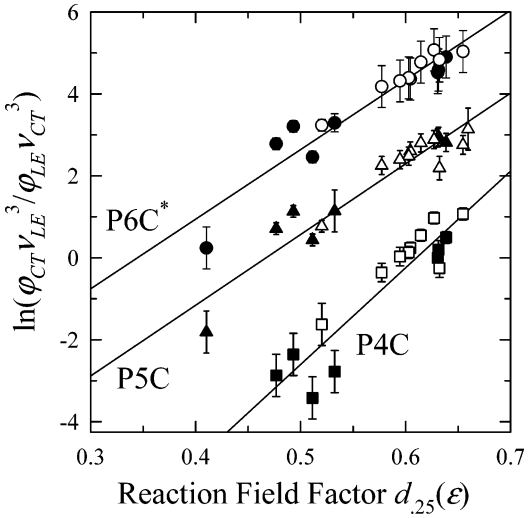

Figure 5. CT/LE emission intensity ratio of P4C (squares), P5C (triangles), and P6C (circles) plotted against the reaction field factor $d_c(\epsilon)$ ($c = 0.25$). The intensity ratio is plotted in a logarithmic format and the frequency factors are included so that the quantity plotted is proportional to K_{eq} (see text). The P6C data have been shifted by +1 unit on the y axis for clarity. Filled and open symbols denote aprotic and protic solvents, respectively. Data in benzene and dioxane are excluded from these plots.

and 5. Regression coefficients obtained from fitting observed quantities A to the relation $A(\epsilon) = a_0 + a_1 d_c(\epsilon)$ are provided for all three choices of c in Table S5 of the Supporting Information. Note that in these figures and regressions (and subsequent dielectric modeling) two of the solvents listed in Table 1, benzene and dioxane, have been excluded. Because these two solvents possess substantial quadrupole moments but no dipole moment, their solvating characteristics cannot be modeled on the basis of their dielectric constants.

From Figure 4 one sees that the absorption, LE, and CT emission frequencies can each be reasonably approximated as linear functions of $d_{0.25}(\epsilon)$, albeit not to within uncertainties. Apart from ν_{CT} of P4C, which is poorly determined, the slopes of the corresponding frequencies of all of the PnC solutes and, where applicable, of ABN, are comparable. These similar slopes will be interpreted in terms of similar dipole moments of the S_0, LE, and CT states in section VI.

In Figure 5 we correlate the ratios of the CT and LE band areas (or quantum yields φ), in the form

$$\ln\left(\frac{\varphi_{CT}}{\nu_{CT}^3}\frac{\nu_{LE}^3}{\varphi_{LE}}\right) \cong \ln K_{eq} + \text{const} \qquad (4.2)$$

to $d_c(\epsilon)$. As indicated by eq 4.2, this ratio, when normalized by ν^3 to account for radiative rate differences, is expected to be proportional to the equilibrium constant K_{eq} for the LE-CT reaction in the limit of rapid equilibrium (see eq 3.8). The free energy change for the reaction is expected to be proportional to the logarithm of this quantity. Figure 5 illustrates the fact that this measure of the driving force for reaction is also reasonably correlated by solvent dielectric properties. In this case the solvent dependence (slope) is identical in P5C and P6C but appears to be significantly different in P4C. It is worth reiterating with respect to both Figures 4 and 5 that there appears to be nothing in these dielectric correlations of steady-state characteristics to indicate a distinction between the behavior of any of the solute in protic (open symbols) versus aprotic (filled) solvents. As will be discussed in section V and VII, significant differences are found when kinetics are considered.

V. Quantum Yields and Transition Moments

Useful to the interpretation of the spectroscopy of these molecules is an understanding of the radiative rates or transition dipole moments of the states involved. For this reason we have measured quantum yields, lifetimes, and radiative rates of the four solutes in a series of solvents. The data are collected in Table 3. Note that some kinetic data are needed here to derive information about the transition strengths. These data will be discussed in more detail in section VII. The quantum yields φ_{em} listed in Table 3 refer to the entire LE + CT emission. The LE lifetime $\langle\tau_{LE}\rangle$, in the presence of LE−CT interconversion is the average time $\langle\tau_{LE}\rangle = \Sigma_i a_i\tau_i/\Sigma_i a_i$ obtained from multi-exponential fits. Using these quantities, the radiative rate of the LE state is given by[59]

$$k_{LE}^{rad} = \frac{\varphi_{LE}}{\langle\tau_{LE}\rangle} \qquad (5.1)$$

k_{LE}^{nr} in Table 4 denotes the net nonradiative rate, i.e., the rate including reaction, $k_{LE}^{nr} = (1 - \varphi_{LE})/\langle\tau_{LE}\rangle$. Assuming rapid LE

TABLE 3: Radiative Rates and Transition Moments[a]

solvent	φ	$\varphi_{CT}/\varphi_{LE}$	$\langle\tau_{LE}\rangle$/ns	$k_{LE}^{rad}/10^7$ s^{-1}	$k_{LE}^{nr}/10^9$ s^{-1}	$k_{CT}^{rad}/10^7$ s^{-1}	M_{LE}/D	M_{CT}/D	M_{abs}/D
					ABN				
cyclohexane	0.12	~0	4.3	2.7 ± 0.3	0.20 ± 0.02		1.1 ± 0.1		4.0 ± 0.4
methyl acetate	0.094	~0	3.1	3.1 ± 0.3	0.30 ± 0.03		1.3 ± 0.1		4 ± 1
acetonitrile	0.111	~0	2.8	3.9 ± 0.4	0.31 ± 0.04		1.5 ± 0.1		4.5 ± 0.3
methanol	0.024	~0	0.57	4.2 ± 0.5	1.7 ± 0.2		1.6 ± 0.1		4.9 ± 0.3
							1.3		***4.5***
					P4C				
cyclohexane	0.15	~0	3.6	4.2 ± 0.5	0.23 ± 0.03		1.4 ± 0.1		4.7 ± 0.4
methyl acetate	0.090	0.04	2.1	4.0 ± 0.5	0.43 ± 0.05	0.4 ± 1	1.6 ± 0.1	.7 ± 1	
acetonitrile	0.032	0.39	0.55	4.2 ± 0.5	1.8 ± 0.2	0.4 ± 0.2	1.7 ± 0.1	.7 ± 0.2	5.1 ± 0.4
methanol	0.016	0.93	0.14	6 ± 2	7 ± 2	0.43 ± 0.11	2.0 ± 0.3	.8 ± 0.1	5.4 ± 0.8
							1.6	***0.8***	***5.1***
					P5C				
cyclohexane	0.16	~0	3.6	4.3 ± 0.5	0.23 ± 0.03		1.4 ± 0.1		4.9 ± 0.3
methyl acetate	0.028	1.4	0.36	3.2 ± 0.6	2.8 ± 0.5	0.6 ± 0.1	1.4 ± 0.1	1.0 ± 0.1	
acetonitrile	0.016	7.2	0.09	2 ± 1	11 ± 6	0.51 ± 0.08	1.2 ± 0.**3**	0.9 ± 0.1	5.2 ± 0.4
methanol	0.007	6.1	0.024	4.0 ± 0.8	42 ± 8	0.43 ± 0.07	1.6 ± 0.2	0.9 ± 0.1	5.4 ± 0.4
							1.4	***0.9***	***5.2***
					P6C				
cyclohexane	0.086	~0	2.3	3.8 ± 0.4	0.40 ± 0.04		1.4 ± 0.1		4.2 ± 0.4
methyl acetate	0.028	5.0	0.26	1.8 ± 0.4	3.9 ± 0.9	0.86 ± 0.12	1.1 ± 0.1	1.0 ± 0.1	
acetonitrile	0.020	17	0.062	1.8 ± 0.5	16 ± 5	0.64 ± 0.08	1.2 ± 0.2	1.0 ± 0.1	5.1 ± 0.4
methanol	0.011	25	0.036	1.2 ± 0.6	28 ± 13	0.56 ± 0.07	.9 ± 0.2	1.0 ± 0.1	5.0 ± 0.3
							1.3	***1.0***	***4.8***

[a] φ is the total emission quantum yield (±10%), $\varphi_{CT}/\varphi_{LE}$ the ratio of band areas (±15%) and $\langle\tau_{LE}\rangle$ the average LE decay time $\langle\tau_{LE}\rangle = \Sigma_i a_i\tau_i/\Sigma_i a_i$. (With the exception of the single-exponential decays observed for ABN in all solvents and the PnC compounds in cyclohexane, the LE emission is at least biexponential, as described in section VII.) k_x^{rad}, k_x^{nr}, and M_x are the radiative and nonradiative rate constants and transition dipole moments associated with emission from state x (eqs 5.1−5.3). M_{abs} is the net ($S_0 \rightarrow L_a + L_b$) absorption transition moment (eq 5.4). Values in italics below the M_x are weighted averages.

TABLE 4: Dipole Moments Estimated from Simple Solvatochromic Analysis[a]

dipole	observable	a = 4.6 Å	a = 3 Å	a = 4 Å	a = 5 Å	α = 0	$\mu^*(\infty)$
μ_a^{LE}	ν_{abs}	13.2	8.5	11.0	15.0	15.2	17.6
μ_{LE}	ν_{LE}	10.3	8.0	9.3	11.1	11.2	13.7
μ_{CT}	ν_{CT}	15.1	9.4	12.8	16.7	18.5	20.1
μ_{CT}	ϕ_{rat} ($+\nu_{LE}$)	13.4	9.1	11.6	14.7	15.7	17.9

[a] Dipole moments (D) estimated using the average slopes from Table S5 (Supporting Information) and the formalism of eqs 6.18−21. The first four columns of numbers are calculated using $\alpha/a^3 = 0.25$ and the cavity radii a indicated. In the column labeled "$\alpha = 0$" are values determined using a cavity radius of 4.6 Å and assuming the solute to be nonpolarizable. The final column lists values of the solution-phase dipole moments corresponding to the $a = 4.6$ Å gas-phase results ($\alpha/a^3 = 0.25$) and for the limiting case $\epsilon \rightarrow \infty$ according to the relation $\tilde{\mu}(\infty) = \mu/\{1 - 2\alpha/a^3\}$. The μ_{CT} values in the last row are derived from CT/LE intensity ratios using eqs 6.21 and the μ_{LE} values obtained from the ν_{LE} data.

↔ CT equilibrium, eq 3.8 provides the radiative rate of the CT state as

$$k_{CT}^{rad} \cong \varphi_{CT} k_{dec}(1 + K_{eq}^{-1}) \tag{5.2}$$

Values of $k_{dec} = \tau_{dec}^{-1}$ and K_{eq} used for these calculations are listed later in Tables 8 and 9 of sectionVII. We note that other workers have typically deduced values of k_{CT}^{rad} assuming that the K_{eq}^{-1} term in eq 5.2 is negligible.[60] This assumption is reasonable in all of the cases in Table 3 except for P4C in methyl acetate, where the correction amounts to a factor of 3.

Quantum yields and radiative rates for the nonreactive molecule ABN have been previously measured in a number of room-temperature solvents. Values of k_{LE}^{rad} (in units of 10^7 s^{-1}) of 2.8 in *n*-hexane[61] and cyclohexane,[62] 3.8 and 3.9 in 2-methylpentane and hexadecane[63] and 3.7, 3.9, and 4.6 in benzene, dioxane, and acetonitrile[62] are consistent with the values determined here. No determinations of k_{LE}^{rad} have been made for the other compounds, but comparable values ((3.9−5.4) × 10^7 s^{-1}) have been reported for DMABN in various nonpolar solvents.[63,64] The radiative rates of the CT states of P5C and P6C have been previously reported to be 1.0 × 10^7 and 1.6 × 10^7 s^{-1} in 1-chlorobutane, respectively.[11] These rates are considerably larger than the values determined here, 0.6 × 10^7 and 0.9 × 10^7 s^{-1} in methyl acetate, a solvent of comparable polarity to chlorobutane. Better agreement is found for k_{CT}^{rad} of P4C (0.4 × 10^7 s^{-1}) for which the literature value of 0.54 × 10^7 s^{-1} in acetonitrile was previously reported.[19]

Transition dipole moments of the radiative transitions, M_x, can be determined from the radiative rate data according to[65]

$$M_x^2 = \frac{3hc^3}{64\pi^4} \frac{k_x^{rad}}{n^3 \tilde{\nu}_x^3} \tag{5.3}$$

which we evaluate using[66]

$$M_x/\mathrm{D} = 1785.7 \left(\frac{k_x^{rad}/\mathrm{s}^{-1}}{n^3(\tilde{\nu}_x^3/\mathrm{cm}^{-3})} \right)^{1/2} \tag{5.4}$$

where n is the solvent refractive index and $\tilde{\nu}_x^3 = \int F_x(\nu)\, d\nu / \int F_x(\nu)\nu^{-3}\, d\nu$ with $F_x(\nu)$ denoting the fluorescence spectrum of species x = LE or CT.

The LE transition moments are of similar magnitude in all four compounds, indicating LE states of similar character. For these DMABN-like solutes, the LE state is expected to be mainly of L_b character,[1] consistent with the modest magnitude of M_{LE} found here. In the case of ABN and P4C there appears to be a significant (35−40%) increase of M_{LE} with increasing solvent

polarity. A possible explanation for this observation is the presence of enhanced mixing (intensity borrowing) from the higher-lying but more polar ^1L_a state, brought about by increasing solvent polarity. In P5C and P6C, on the other hand, M_{LE} does not display any clear trend with solvent polarity. The CT transition moments are all smaller than the LE moments, but by less than a factor of 2. (The much larger difference between the radiative rates of the CT and LE displayed in Table 3 is mainly due to the lower frequencies of the CT emission.) The CT transition moments are all on the order of 1 D, far from what would be considered a forbidden transition (i.e., from what is expected for a transition between orthogonal π orbitals). These moments increase slightly in the order P4C < P5C < P6C. More interestingly, the values of M_{CT} exhibit no clear dependence on solvent polarity. This last observation is consistent with the results reported by Okada et al.[67] who found M_{CT} to fall between 1.1 and 1.3 D in DMABN and 0.6−0.7 D in 6-cyanobenzquinuclidine in a set of 11 solvents of varying polarity. This constancy implies that the character of the CT emitting state is approximately independent of solvent polarity. The magnitude of M_{CT} as well as its solvent independence is surprising and has important implications for modeling the spectra of these compounds, as will be discussed later in section VI.

For comparison to the emission moments, we also list values of the "net absorption transition moments" of the composite ($S_0 \rightarrow L_a + S_0 \rightarrow L_b$) absorption bands, determined according to[65,66]

$$M_{abs}{}^2 = \frac{3hc}{8\pi^3}\frac{\ln(10)}{N_A}\frac{1}{n}\int_{abs}\frac{\epsilon(\nu)}{\nu}\,d\nu \tag{5.5}$$

and

$$M_{abs}/D = 9.584 \times 10^{-2}\frac{1}{n}\int_{abs}(\epsilon(\nu)/M^{-1}\,cm^{-1})\frac{d\nu}{\nu} \tag{5.6}$$

where $\epsilon(\nu)$ is the molar decadic extinction coefficient. These values appear to increase slightly with increasing solvent polarity, by an average of ∼15% between cyclohexane and methanol. The origins of this increase are unknown. The solvent-averaged values of M_{abs} are similar in all of the solutes, $M_{abs} \sim$ 4.9 D. Although it is impossible to accurately separate the L_a and L_b contributions to the absorption, a reasonable estimate is that the fractional intensity contributed by the L_b transition is between 10 and 30% of the total intensity (based on attempts to decompose line shapes as illustrated in the top panel of Figure 1). Such a dissection would imply individual transition moments of $M_{0\rightarrow b} = 1.5-2.6$ D and $M_{0\rightarrow a} = 4.1-4.6$ D for independent component transitions. Comparing these values to the values of 1.3−1.6 D found for M_{LE} confirms that the assignment of the LE state as being primarily of L_b character.

VI. Modeling the Solution-Phase Energies and Spectra

As a framework for interpreting the solvatochromism described in section IV, we consider a 2-dimensional model for how the energies of the relevant electronic states depend on solvent. Our formulation is based on the theoretical treatments of TICT reactions by Kim and Hynes[43,45,68] and is also similar to those employed by other workers.[39,40,46] In the spirit of the Marcus model of electron transfer, we assume that the free energies of the diabatic electronic states G_i in the problem are parabolic in the solvation coordinate $\vec{\mu}_s$. They also depend on some nuclear coordinate of the solute, here assumed to be primarily the amino twist angle θ:

$$G_i(\theta,\vec{\mu}_s) = U_i(\theta) - {}^1/_2(B_{el}^{(i)} + B_{nuc}^{(i)})\mu_i(\theta)^2 + {}^1/_2B_{nuc}^{(i)}\{\vec{\mu}_i(\theta) - \vec{\mu}_s\}^2 \tag{6.1}$$

In this equation $U_i(\theta)$ and $\vec{\mu}_i(\theta)$ denote the θ-dependent gas-phase energy and dipole moment of solute electronic state i, and $B_{el}^{(i)}$ and $B_{nuc}^{(i)}$ are the electronic and nuclear polarizabilities of the solvent. As suggested by van der Zwan and Hynes,[69] we describe the solvation coordinate (or solvent polarization) by a dipole moment $\vec{\mu}_s$. That is, the *solvent* polarization is measured by specifying the value of the *solute* dipole moment with which it would be in equilibrium. The terms $B_{el}^{(i)}$ and $B_{nuc}^{(i)}$ partition the total polarizability of the solvent into components that are faster ($B_{el}^{(i)}$) and slower ($B_{nuc}^{(i)}$) than the solute electronic transition. For these functions we adopt the standard dielectric continuum descriptions,[69,70]

$$B_{el}^{(i)} = \frac{2}{a^3}\frac{d_0(n^2)}{1 - 2(\alpha_i/a^3)d_0(n^2)} \tag{6.2}$$

and

$$B_{nuc}^{(i)} = B_{tot}^{(i)} - B_{el}^{(i)} \tag{6.3}$$

with

$$B_{tot}^{(i)} = \frac{2}{a^3}\frac{d_0(\epsilon)}{1 - 2(\alpha_i/a^3)d_0(\epsilon)} \tag{6.4}$$

and

$$d_0(x) \equiv \frac{x-1}{2x+1} \tag{6.5}$$

Equations 6.2−6.5 result from modeling the solute as a polarizable point dipole (of polarizability α) centered inside a spherical cavity of radius a, and the solvent as a continuous fluid with refractive index n and static dielectric constant ϵ. The solutes considered here are not spherical in shape, nor is their charge distribution well represented by a point dipole. However, it is not unreasonable to expect that the solvent dependence embodied in eqs 6.2−4 is still appropriate. In this sense, the coupling factors μ^2/a^3 that are derived by fitting experimental data to these relations should be viewed as effective values, which incorporate both the nonspherical shape and the distributed nature of the solute charge distribution.

We assume the spectroscopically relevant states to be composed of three diabatic states: the ground state, S_0, and the two close-lying excited states L_b and L_a. The energies of the diabatic states are assumed to be described by eq 6.1 with appropriate values of $U_i(\theta)$ and $\vec{\mu}_i(\theta)$. The L_b and L_a states are allowed to mix to form the adiabatic states S_1 and S_2 according to

$$\Psi_{S1}(\theta,\vec{\mu}_s) = C\psi_b + (1 - C^2)^{1/2}\psi_a$$
$$\Psi_{S2}(\theta,\vec{\mu}_s) = C\psi_a - (1 - C^2)^{1/2}\psi_b \tag{6.6}$$

where the mixing coefficient is

$$C(\theta,\vec{\mu}_s) = \left(\frac{V_{el}{}^2}{V_{el}{}^2 + [G_b - G_{S1}]^2}\right)^{1/2} \tag{6.7}$$

with the resulting adiabatic-state energies described by

$$G_{S1}(\theta,\vec{\mu}_s) = {}^1/_2\{(G_b + G_a) - \sqrt{(G_b - G_a)^2 + 4V_{el}{}^2}\}$$
$$G_{S2}(\theta,\vec{\mu}_s) = {}^1/_2\{(G_b + G_a) + \sqrt{(G_b - G_a)^2 + 4V_{el}{}^2}\} \quad (6.8)$$

The electronic coupling matrix element V_{el} is assumed to be independent of both θ and $\vec{\mu}_s$. Absorption to both S_1 and S_2 occurs, but emission is assumed to involve only the S_1 state.

Equations 6.1−6.8 provide a unified description of the sort of 2-dimensional solution-phase surfaces responsible for the solvent-dependent spectroscopy and S_1 dynamics of the LE → CT reaction in P*n*C solutes. In future work, we intend to use such surfaces to fit the detailed line shapes of the steady-state absorption and emission spectra, and ultimately, the spectral dynamics observed in these systems. But this is a challenging problem. For now we make only the first step toward this end, by exploring whether such a model can reproduce the solvent dependence of the four characteristics of the steady-state spectra described in section IV: the peak frequencies of the absorption and emission (LE and CT) bands and the ratio of CT/LE emission intensities. For such purposes, a number of simplifications of the basic model are useful. First, we neglect the fact that molecules will be distributed over a range of θ and $\vec{\mu}_s$ values, and consider only energy differences between the important minima (θ_i^*,μ_i^*) on the free energy surfaces and their Franck−Condon projections. So, for example, the LE peak frequency is assumed to be given by

$$h\nu_{LE} = G_1(\theta_{LE}^*,\vec{\mu}_{LE}^*) - G_0(\theta_{LE}^*,\vec{\mu}_{LE}^*) \quad (6.9)$$

where $G_1(\theta_{LE}^*,\vec{\mu}_{LE}^*)$ is the free energy of the S_1 surface at the minimum ascribed to the LE "state" and $G_0(\theta_{LE}^*,\vec{\mu}_{LE}^*)$ is the free energy of the ground-state surface at these same coordinates. To the extent that these minima are well defined, this focus represents only a minor approximation, at least for frequency calculations. To significantly simplify the analysis, more drastic approximations are required, because in general, the value of θ^* will depend on solvent polarity and therefore so will $\vec{\mu}^*$, leading to a highly nonlinear fitting problem. Assuming that the primary internal coordinate of importance is twisting of the amino group, semiempirical calculations of the sort discussed below[71,72] suggest that the minima on the S_0 and S_1 surfaces remain essentially at the extreme values of $\theta \sim 0°$ (S_0 and LE minima) and $\theta \sim 90°$ (CT minimum) for all solutes examined except P6C.[22] In the latter case, calculations estimate $\theta \sim 30°$ for the S_0 and LE minima due to steric effects both in the gas phase[22,24] and in solution.[71] It is therefore reasonable to adopt solvent-independent values for the free energy minima $\theta_0^* = \theta_{LE}^* \equiv \theta_{LE}$ and $\theta_{CT}^* \equiv \theta_{CT}$, which leads to solvent-independent values for the dipole moments of the diabatic states: $\vec{\mu}_0^*(\theta_0^*) = \vec{\mu}_0^*(\theta_{LE}^*) \equiv \mu_0$, $\vec{\mu}_0^*(\theta_{CT}^*) \equiv \mu_0^{CT}$, $\vec{\mu}_{a,b}^*(\theta_{LE}^*) \equiv \mu_{a,b}^{LE}$, and $\vec{\mu}_{a,b}^*(\theta_{CT}^*) \equiv \mu_{a,b}^{CT}$. We henceforth also drop the vector notation for the dipole moments, assuming all dipoles to be collinear. In this case the various transition frequencies can be simply expressed

$$h\nu_{abs} \cong G_a(\theta_{LE},\mu_0) - G_0(\theta_{LE},\mu_0) \quad (6.10)$$

$$h\nu_{LE} \cong G_1(\theta_{LE},\mu_{LE}^*) - G_0(\theta_{LE},\mu_{LE}^*) \quad (6.11)$$

$$h\nu_{CT} \cong G_1(\theta_{CT},\mu_{CT}^*) - G_0(\theta_{CT},\mu_{CT}^*) \quad (6.12)$$

where $\mu_{LE}^* = \mu_{LE}^*(\theta_{LE})$, etc., and the "*" designation indicates that μ_{LE} and μ_{CT} are still solvent-dependent due to the solvent dependence of the $L_a - L_b$ mixing. In eq 6.10 we have taken the final state of the absorption to be the L_a diabatic state in recognition of the fact that the peak frequencies measured in experiment correspond to the stronger L_a ($\sim S_2(\theta_{LE})$) transition. Finally, in the rapid equilibrium limit, the ratio of CT to LE emission intensities can be written

$$\ln(\phi_{CT}/\phi_{LE}) \cong \ln(K_{eq}) + \ln(k_{CT}^{rad}/k_{LE}^{rad})$$
$$\cong \{G_1(\theta_{CT},\mu_{CT}^*) - G_1(\theta_{LE},\mu_{LE}^*)\}/k_BT + \ln(M_{CT}{}^2\nu_{CT}{}^3/M_{LE}{}^2\nu_{LE}{}^3) \quad (6.13)$$

where M_{CT} and M_{LE} are the transition moments of the CT and LE states, assumed to be determined from the transition moments between the ground and the perpendicularly polarized L_b and L_a states, M_b and M_a, by

$$M_{CT}{}^2 \equiv M_1{}^2(\theta_{CT}) = C^2|M_b^{CT}|^2 + (1 - C^2)|M_a^{CT}|^2 \quad (6.14)$$

$$M_{LE}{}^2 \equiv M_1{}^2(\theta_{LE}) = C^2|M_b^{LE}|^2 + (1 - C^2)|M_a^{LE}|^2 \quad (6.15)$$

VI-A. Further Simplifications and Initial Fits. Before fitting to the model just described, it is useful to see how the correlations with the dielectric function $d_c(\epsilon)$ displayed in Figures 4 and 5 come about. Simplified predictions for the frequencies and band ratios can be obtained by making the further assumption that solvent-dependent mixing of the states L_b and L_a is not important near the LE and CT minima. In this case all relevant dipole moments become constants and one obtains the sort of solvatochromic equations often used to analyze CT spectra. For example, assuming that the LE state is of purely L_b character in any solvent, $\mu_{LE}^* \cong \mu_b(\theta_{LE}) \equiv \mu_{LE}$, the LE frequency (eq 6.11) can be rewritten

$$h\nu_{LE} \cong G_b(\theta_{LE},\mu_{LE}) - G_0(\theta_{LE},\mu_{LE})$$
$$= \{U_b^{LE} - {}^1/_2B_{tot}^{(b)}\mu_{LE}{}^2\} - \{U_0^{LE} - {}^1/_2B_{tot}^{(0)}\mu_0{}^2 + {}^1/_2B_{nuc}^{(0)}(\mu_0 - \mu_{LE})^2\} \quad (6.16)$$

Two further simplifications can be used to cast this equation into a more transparent form. First, we assume that the solute polarizabilities are the same in all three diabatic states and related to the solute size by $\alpha_i = \alpha = ca.^3$ In this case the B terms become state-independent and can be written $B_{el} = 2a^{-3}d_c(n^2)$, $B_{nuc} = B_{tot} - B_{el}$, and $B_{tot} = 2a^{-3}d_c(\epsilon)$ with $d_c(x)$ given by eq 4.1. The LE frequency is then

$$h\nu_{LE} \cong h\nu_{LE}^0 - A_{LE}d_c(n^2) - C_{LE}d_c(\epsilon) \quad (6.17)$$

where $h\nu_{LE}^0 \equiv U_b^{LE} - U_0^{LE}$, $A_{LE} = a^{-3}(\mu_{LE} - \mu_0)^2$, and $C_{LE} = 2a^{-3}\mu_{LE}(\mu_{LE} - \mu_0)$. Second, over the range of solvents considered here, the relative variations in $d_c(\epsilon)$ are 3−4 times larger than the relative variations in $d_c(n^2)$ so that to a reasonable approximation the second term in eq 6.17 can be considered solvent-independent. This approximation provides

$$h\nu_{LE} \cong \text{const} - C_{LE}d_c(\epsilon) \quad \text{with} \quad C_{LE} = 2a^{-3}\mu_{LE}(\mu_{LE} - \mu_0) \quad (6.18)$$

Similar reasoning leads to

$$h\nu_{abs} \cong \text{const} - C_{abs}d_c(\epsilon) \quad \text{with} \quad C_{abs} = 2a^{-3}\mu_0(\mu_a^{LE} - \mu_0) \quad (6.19)$$

Assuming that the CT state is primarily of L_a character and denoting $\mu_{CT}^* \cong \mu_a(\theta_{CT}) \equiv \mu_{CT}$ leads to the expression

$$h\nu_{CT} \cong \text{const} - C_{CT}d_c(\epsilon) \quad \text{with}$$
$$C_{CT} = 2a^{-3}\mu_{CT}(\mu_{CT} - \mu_0^{CT}) \quad (6.20)$$

Finally, the quantum yield ratio from eq 6.13 becomes

$$\ln(\phi_{CT}\nu_{LE}^3/\phi_{LE}\nu_{CT}^3) \cong \text{const} + C_\phi d_c(\epsilon) \quad \text{with}$$
$$C_\phi \cong a^{-3}\{\mu_{CT}^2 - \mu_{LE}^2\}/k_BT \quad (6.21)$$

Thus, to a reasonable first approximation, the model described in section VI is expected to lead to linear relationships between the various frequencies and quantum yield ratios and the total solvent polarity as measured by $d_c(\epsilon)$. The slopes of the best fit linear relations to these data therefore provide information about the relative dipole moments of the states.

In Table 4 we interpret the solute-averaged values of the slopes from the solvatochromic fits in this manner. Using representative values for the ground-state dipole moments, $\mu_0 = 6.7$ D and $\mu_0^{CT} = 4.9$ D, derived from electronic structure calculations discussed later, and a cavity radius of 4.6 Å, the dipole moments listed under the column labeled "$a = 4.6$ Å" are obtained. This particular choice of cavity radius will also be justified in the following section. For now, we note that the dipole moments derived from this analysis are rather sensitive to the value of a, as indicated by the results for the alternative choices also listed. The variation of ±50% in the dipole values for reasonable values of a illustrated in Table 4 underscores the well-known ambiguities in determining dipole moments from solvatochromic data.

The derived dipole moments also depend on the choice of solute polarizability. In the first four sets of values listed in Table 4 we have assumed the choice $\alpha_i = \alpha = 0.25a^3$, i.e., $c = 0.25$ in eq 4.1 The column labeled "$\alpha = 0$" in Table 4 gives the results obtained assuming the solute to be nonpolarizable, which corresponds to the most often used reaction field factor $d_0(\epsilon) = (\epsilon - 1)/(2\epsilon + 1)$. In this case, the dipole moments are much larger. However, the dependence of μ on α is partly a matter of perspective. The reason is that the dipole moments μ listed in Table 4 are intrinsic or "gas-phase" values. In solution, these dipole moments are enhanced by the effect of solvent polarization, such that the solution-phase moments $\tilde{\mu}$ are given by[70]

$$\tilde{\mu}(\epsilon) = \mu/\{1 - 2d(\epsilon)\alpha/a^3\} \quad (6.22)$$

For the choice $\alpha/a^3 = 0.25$ adopted here, the solution-phase dipole moments are enhanced by a factor of $^4/_3$ as $\epsilon \rightarrow \infty$. These latter values are listed as $\tilde{\mu}(\infty)$ in Table 4. Comparing such dipole moments with the values deduced using a nonpolarizable reaction field shows that the $\alpha = 0$ values reflect a compromise between the gas-phase and $\epsilon \rightarrow \infty$ values of the polarizable solute.

Despite the uncertainties in the quantitative determination of dipole moments, the qualitative trends are clear. Using only the frequency shift data, one finds a consistent ordering of dipole moments, $\mu_0 < \mu_{LE} < \mu_a^{LE} < \mu_{CT}$. The change between the ground and LE states is far from small (3.6 D) and is in fact comparable to the difference between the LE and CT states (4.8 D). Thus, the charge distribution of the LE state is not particularly close to that of the S_0 state. Moreover, the absorption data indicate that the $L_a(\theta_{LE})$ state is nearly as polar as the CT

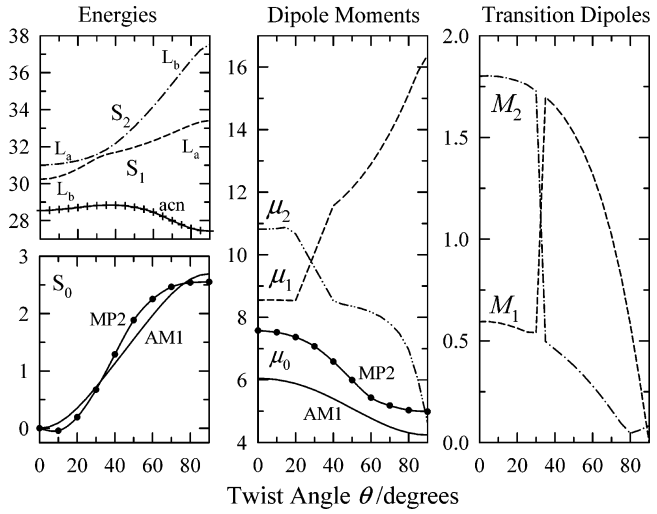

Figure 6. Optimized energies (10^3 cm^{-1}), dipole moments (D), and transition dipole moments (D) of the S_0 (solid), S_1 (dashed), and S_2 (dot−dash) states of P5C as a function of twist angle θ, derived from AM1/CI calculations. The curves labeled MP2 show the S_0 results using the MP2/6-31G(d)//RHF/6-31G(d) method. The curve labeled "acn" (+ symbols) is the S_1 curve predicted for acetonitrile solution by an AM1/CI self-consistent reaction field calculation (see text).

($L_a(\theta_{CT})$) state, meaning that much of the charge transfer that accompanies the LE → CT reaction does not require solute nuclear reorganization. These observations are not new to the present study. The dipole moments listed in Table 4 fall within the range of literature estimates for DMABN and related compounds.[1] However, the large polarity change between S_0 and the LE states, and the similarity between μ_a^{LE} and μ_{CT}, are typically not stressed in qualitative discussions of these reactions.

A problematic aspect of the above analysis is that the difference between μ_{LE} and μ_{CT} is predicted to be smaller when using information about CT/LE intensity ratios than when μ_{CT} is derived from frequency shift data. This inconsistency can be seen by comparing the values of μ_{CT} in the last two rows of Table 4. For later reference, we note that the relative difference in the two values of μ_{CT} is much smaller for the smallest cavity radius and much larger for a nonpolarizable solute than for the preferred model. At this juncture it is not clear whether this inconsistency reflects a failure of the basic model or whether it is due to some of the simplifications made here for convenience. We therefore next consider a more complete model analysis of the experimental data.

VI-B. Electronic Structure Calculations and Complete Model Fits. Even with the simplifications described by eqs 6.10−13, complete specification of the model embodied in eqs 6.1−8 requires a total of 21 solute parameters. But Figures 4 and 5 demonstrate that all of the spectral features of interest here can be reasonably described as linear functions of a single solvent variable. Thus, no more than eight independent solute parameters (the slopes and intercepts of these correlations) should be needed to model the data for a given solute. To achieve meaningful fits to the solvatochromic data, it is therefore necessary to fix most of the model parameters in some way. We do so with the help of electronic structure calculations, briefly described below.

We have performed gas-phase calculations of all of the solutes as functions of twist angle θ at the MP2/6-31G(d)//RHF/6-31G(d,p) level for the ground state and at the semiempirical AM1/CI level for the first few excited states. Examples of such calculations are shown in Figure 6, where we plot the energies, dipole moments, and transition dipole moments calculated for

the S_0, S_1, and S_2 states of P5C. The AM1/CI calculations predict the S_1 state to be of L_b character near $\theta = 0°$ and of L_a character near $\theta = 90°$. We find similar behavior in the other P*n*C molecules, as well as in the previously studied case of DMABN.[72] In P5C, the two diabatic states cross near $\theta = 30°$, which results in abrupt changes in the dipole and transition moments of the adiabatic S_1 and S_2 states near this value of θ. On the basis of a generalized Marcus−Hush treatment,[73] the L_b−L_a coupling V_{el} is calculated to be about 100 cm^{-1} in this system. In the gas phase, the 90° (θ_{CT}) states of all of the solutes are predicted to lie at higher energies than the θ_{LE} states. The situation is different in solution, as illustrated by the curve labeled "acn" in Figure 6. This curve is the energy of the S_1 state in acetonitrile solution predicted from self-consistent reaction field (SCRF) calculations. In this case the CT (90°, L_a) state is calculated to be a minimum on the S_1 surface and to lie at lower energy than the LE minimum by 1100 cm^{-1} (13 kJ/mol). This difference is quite close to the experimental estimate of 10.0 ± 0.6 kJ/mol (section VII). This example is illustrative of the sort of semiquantitative agreement we often find from such SCRF calculations. As first noted in an early study of related molecules,[72] we find that the predictions of semiempirical SCRF calculations are at least qualitatively consistent with experimental observations for all of the solutes examined here. Also shown in Figure 6 are some results for the S_0 state in the gas phase using more accurate, MP2 calculations. The similarities and differences between the AM1 and MP2 predictions, as well as a variety of other observations, suggest that these semiempirical calculations provide reliable starting points for modeling experimental data, even if they are not completely quantitative.

The calculated properties of the LE and CT states needed for modeling are summarized in Table 5.[74] For the ground state the MP2 calculations are listed as the primary data with corresponding AM1 values in brackets. For the excited states we also list dipole moments available from DFT/MRCI calculations of Parusel[24] in parentheses. From these data one observes that the dipole moments of the P*n*C molecules, and to a lesser extent ABN, are quite similar to one another in each diabatic state. The state energies are also comparable within this series, the most important variation being the systematic decrease in U_a^{CT} with increasing ring size. Comparisons between the AM1 dipole moments and the more accurate calculations indicate that the AM1 values are probably slightly smaller than the correct values. The transition moments in the LE geometries are also all very similar. The calculated values of M_b^{LE} are ∼0.6 D, 2−3-fold smaller than the experimental values of 1.3−1.6 D (Table 3). The net absorption transition moments, estimated from $M_{abs}^2 = (M_b^{LE})^2 + (M_a^{LE})^2 \sim 1.9$ D, are also much smaller than observed values (4−5 D), suggesting that M_a^{LE} is probably also underestimated by a similar factor in these calculations. The greatest variation among the calculated values lies in the transition moments of the CT states. For planar amino groups the transition moments vanish at $\theta = 90°$. Nonzero values of M_b^{CT} or M_a^{CT} therefore indicate where some degree of amino-group pyramidalization is predicted by the calculations.

Effective cavity radii and polarizabilities used for modeling were based on the results of SCRF AM1 calculations as follows. Dipole moments of the various states were calculated at a number of values of θ in the gas phase and in media having dielectric constants of 5 and 30. The enhancements of the dipole moments from the gas phase to these dielectric media ($\tilde{\mu}(\epsilon)/\mu$) were then fit to eq 6.22 to determine the values of the polarizability density α/a^3 listed in Table 5. These values are, to a reasonable approximation, independent of θ. Like the dipole moments, the variations in α/a^3 with solute are not large. There is more variation among the different electronic states, with α/a^3 being largest for the ^1L_b state and smallest for the ^1L_a state. But even here the variations are modest and, to simplify the analysis, we begin by adopting the average value $\alpha/a^3 = 0.30$ for all states and solutes. Effective cavity radii are then determined from this value and the van der Waals volume V_{vdw} of the solute calculated from atom-based increments[75] using the empirical correlation, $\alpha/Å^3 \cong 0.0268(V_{vdw}/Å^3)^{1.35}$.[76] Because the SCRF calculations use a molecularly shaped cavity, these values of a are effective spherical cavity radii, which should provide fitted dipole moments of realistic magnitude. We note that they are all approximately 1 Å larger than the radii calculated directly from the van der Waals volumes, also a sensible result.

TABLE 5: Model Parameters from Electronic Structure Calculations[a]

S_0 State

	$U_0^{CT}/10^3$ cm^{-1}	μ_0/D	μ_0^{CT}/D	α/a^3	$V_{vdw}/Å^3$	r_{vdw}/Å	a/Å
ABN	2.0 [2.0]	6.1 [4.8]	4.7 [3.6]	0.31	112	3.0	3.74
P4C	2.4 [1.4]	6.9 [5.0]	5.0 [3.9]	0.30	152	3.3	4.29
P5C	2.6 [1.1]	6.9 [5.5]	5.0 [3.9]	0.32	169	3.4	4.50
P6C	0.8 [0.8]	6.8 [5.4]	4.9 [3.9]	0.32	186	3.5	4.69

^1L_b State

	$U_b^{LE}/10^3$ cm^{-1}	$U_b^{CT}/10^3$ cm^{-1}	μ_b^{LE}/D	μ_b^{CT}/D	M_b^{LE}/D	M_b^{CT}/D	α/a^3
ABN	29.8	39.2	6.6	4.5	0.54	0.12	0.33
P4C	31.2	37.4	8.5 (9.0)	4.7 (5.6)	0.65	0.00	0.39
P5C	30.5	37.5	8.6 (9.8)	4.6 (5.9)	0.63	0.08	0.33
P6C	30.7	36.2	8.5 (9.3)	5.7 (5.4)	0.60	0.23	0.33

^1L_a State

	$U_a^{LE}/10^3$ cm^{-1}	$U_a^{CT}/10^3$ cm^{-1}	μ_a^{LE}/D	μ_a^{CT}/D	M_a^{LE}/D	M_a^{CT}/D	α/a^3
ABN	32.0		8.5		1.7		0.31
P4C	31.9	35.2	9.9 (13.0)	16.1 (16.9)	1.9	0.00	0.27
P5C	31.2	33.7	10.8 (13.7)	16.4 (17.7)	1.9	0.00	0.25
P6C	31.7	33.2	10.7 (13.2)	16.6 (18.1)	1.7	0.12	0.26

[a] LE and CT refer to the twist angle corresponding to the assumed minima on the S_1 potential surface. In the gas phase there is always an LE minimum in S_1 near the S_0 minimum (usually $\theta \sim 0°$). The "CT" state refers to $\theta = 90°$, which is often an S_1 minimum in polar solvents but is a maximum in the gas phase. Energies U are measured relative to the S_0 minimum. V_{vdw} is the van der Waals volume determined from volume increments,[75] r_{vdw} the radius of a sphere of this volume, and a the cavity radius used for modeling (see text). Ground-state properties are from MP2/6-31G(d)//RHF/6-31G(d,p) calculations. Excited-state properties are from AM1/CI calculations. In all cases energies were minimized with respect to all coordinates with the possible exception of the twist angle at the CT geometry. LE minima were located at $\theta = 0°$ with the exception of P6C where the minimum in both the ground and LE states is at $\theta \sim 30°$. Ground-state values in brackets are the corresponding AM1/CI values. Excited-state dipole moments in parentheses are from the DFT/MRCI calculations of Parusel.[24]

We now return to the problem of fitting the solvatochromic data. Most of the 21 parameters upon which the model depends can be fixed using either the calculation results just described or experimental data. These fixed parameters are listed in Table 6A. The ground-state properties $U_0^{LE} \equiv 0$, U_0^{CT}, $\mu_0^{LE} \equiv \mu_0$, and μ_0^{CT} are the MP2-calculated values. Of the four transition moments M_b^{LE}, M_b^{CT}, M_a^{LE}, and M_a^{CT}, only the ratio $M_{CT}/M_{LE} \cong M_a^{CT}/M_b^{LE}$ affects the CT/LE quantum yield ratios examined here. The solute-averaged values $M_b^{LE} \cong 1.4$ D, $M_a^{LE} \cong 5$ D

TABLE 6: Solvatochromic Model Fits[a]

A. Fixed Parameters

	a/Å	$U_0^{CT}/10^3$ cm^{-1}	μ_0/D	μ_0^{CT}/D	M_a^{CT}/D	solute-independent values
ABN	3.74	1.99	6.12	4.66	- -	$\alpha_0 = \alpha_b = \alpha_c = 0.30a^3$
P4C	4.29	2.41	6.92	4.95	0.71	$U_b^{CT} = 38.0 \times 10^3$ cm^{-1}; $\mu_b^{CT} = 4.3$ D
P5C	4.50	2.56	7.57	5.00	0.90	$M_b^{LE} = 1.4$ D; $M_b^{CT} = 0.1$ D; $M_a^{LE} = 5.0$ D
P6C	4.69	0.25	6.82	4.87	1.11	$V_{el} = 125$ cm^{-1}; $U_0^{LE} \equiv 0$

B. Fitted Parameters

	N_{free}	χ_ν^2	$U_b^{LE}/10^3$ cm^{-1}	μ_b^{LE}/D	$U_a^{LE}/10^3$ cm^{-1}	$U_a^{CT}/10^3$ cm^{-1}	μ_a^{LE}/D	μ_a^{CT}/D		
			Fit #1: a and α/a^3 Fixed; (a) Frequencies Only Fit						(b) All Data	
ABN	31	2.1	32.0	8.5	39.6		10.0		N_{free}	χ_ν^2
P4C	53	1.8	30.2	9.7	36.9	30.1	11.3	12.8	69	6.2
P5C	56	2.3	30.3	10.4	36.8	31.8	12.9	14.5	74	12.2
P6C	53	2.0	29.4	10.3	36.2	30.2	12.2	15.4	70	12.6
deviation			0%	21%	7%	−1%	16%	−13%		
			Fit #2: a Fixed; $\alpha_b/a^3 = 0.3$, $\alpha_a/a^3 = 0.1$, α_0/a^3 Varied						α_0/a^3	
ABN	33	1.8	32.0	8.8	40.8		13.3		(0.40)	
P4C	68	2.6	30.2	10.1	38.1	34.0	15.3	15.9	0.43	
P5C	73	2.6	30.3	10.7	38.0	32.7	17.3	15.9	0.42	
P6C	69	2.7	29.4	10.9	37.9	31.5	18.6	16.3	0.57	
deviation			10%	26%	10%	5%	61%	−2%		
			Fit #3: α/a^3 Fixed; a Varied						a/Å	
ABN	33	1.9	32.0	7.2	39.4		7.7		(2.75)	
P4C	68	2.3	30.2	7.8	36.7	32.3	8.1	8.8	2.78	
P5C	73	2.5	30.4	8.8	36.6	31.5	9.5	9.8	3.22	
P6C	69	2.0	29.5	7.7	36.0	30.4	7.8	8.3	2.66	
deviation			10%	−1%	7%	1%	−17%	−45%	−36%	

[a] N_{free} is the number of degrees of freedom in the fit and χ_ν^2 is the "goodness-of-fit" statistic.[78] In Fit #1(a), only frequency data and not CT/LE intensity ratios were fit. Values of N_{free} and χ_ν^2 for the case where all data were fit with fixed a and α/a^3 are listed as Fit #1(b). Rows labeled "deviation" are the solute-averaged percent deviations of the fitted parameters from the semiempirical predictions from Table 5.[79] ABN values in parentheses indicate fixed parameters chosen to be similar to the optimized values of the other solutes.

from experiment (Table 3) and $M_b^{CT} \cong 0.1$ D from AM1/CI calculations (Table 5) are used, along with values of M_a^{CT} deduced from the experimental ratios of M_{CT}/M_{LE} (Table 3). Semiempirical calculations such as those in Figure 6 indicate that the $L_b(\theta_{CT})$ state lies much higher in energy than the $L_a(\theta_{CT})$ state and therefore plays no role in determining the properties of the CT state or spectroscopic observables. For this reason U_b^{CT} and μ_b^{CT} are arbitrarily fixed at values of 38 000 cm^{-1} and 4.3 D for all solutes. Finally, V_{el} is fixed at the average calculated value of 125 cm^{-1}. With the above choices of fixed parameters, there remain six others, U_b^{LE}, μ_b^{LE}, U_a^{LE}, U_a^{CT}, μ_a^{LE}, and μ_a^{CT}, which can be varied to fit the experimental data. These fits were carried out with a nonlinear least squares program based on the Marquardt−Levenberg algorithm.[77] The results are detailed in Table 6B.

We first examine the results when only the frequency data ν_{abs}, ν_{LE}, and ν_{CT} are fit. These results are shown as Fit#1(a) in Table 6. Values of the goodness of fit parameter, χ_ν^2,[78] are close to 2 in all cases, indicating reasonable fits to the data. Such values imply a root-mean-square error in the fitted values that is ∼40% larger than the estimated experimental uncertainties. Given the use of a dielectric continuum description for the solvent, closer agreement is not anticipated. The quality of these fits is comparable to, but slightly better than, the individual linear regressions to $d_c(\epsilon)$ shown in Figure 4 (see the χ_ν^2 values in Table S5). The design of the model is such that the three pairs of U_i, μ_i parameters together with the fixed values just suffice to determine the slopes and intercepts of the three frequency correlations shown in Figure 4, so such a correspondence is expected. We note that the fitted dipole moments are also similar to those derived from the preliminary solvatochromic analysis (Table 4 where $\mu_{LE} = \mu_b^{LE}$, $\mu_{CT} = \mu_a^{CT}$), suggesting that the neglect of solvent polarizability variations (n^2 dependence) in the simplified model does little harm. More relevant in assessing the validity of the model is the fact that both the dipole moments and the gas-phase energies are close to the predictions of the AM1/CI calculations. This relationship is quantified in the rows labeled "deviation" in Table 6B, which list solute-averaged values of the relative deviation between the fitted model parameters and their AM1/CI counterparts. The model gas-phase energies[79] U_b^{LE}, U_a^{LE}, and U_a^{CT} are all within 3000 cm^{-1} or 10% of the semiempirical predictions, which is within the accuracy anticipated for the calculated values. The model dipole moments μ_b^{LE} and μ_a^{LE} are ∼20% larger than the AM1/CI values, as are the predictions of higher-level calculations[24] (Table 5), but the dipole moment of the CT state, μ_a^{CT}, is ∼16% smaller than predictions. Overall, the good correspondence between the semiempirical calculations and the solvatochromic analysis provides some confidence in the basic soundness of our description of the excited states.

Unfortunately, when data on the relative intensities of the LE and CT emission bands are included in the analysis, this description exhibits the same inconsistency noted at the end of the previous section. As indicated by Fit #1(b) in Table 6, when frequency and relative intensity data are fit simultaneously, the values of χ_ν^2 increase to 3−6 times larger than values obtained from fits to the frequency data alone. The nature of these poor fits is illustrated by the P6C data in Figure 7. The compromise fit shown here indicates that the model predicts a much greater variation of $\varphi_{CT}/\varphi_{LE}$ with solvent than is observed. The problem is the same one suggested by the preliminary results in Table 4: the 3−5 D difference between μ_b^{LE} and μ_a^{CT} required to fit the solvent dependence of the LE and CT frequencies is larger than needed to fit the solvent dependence

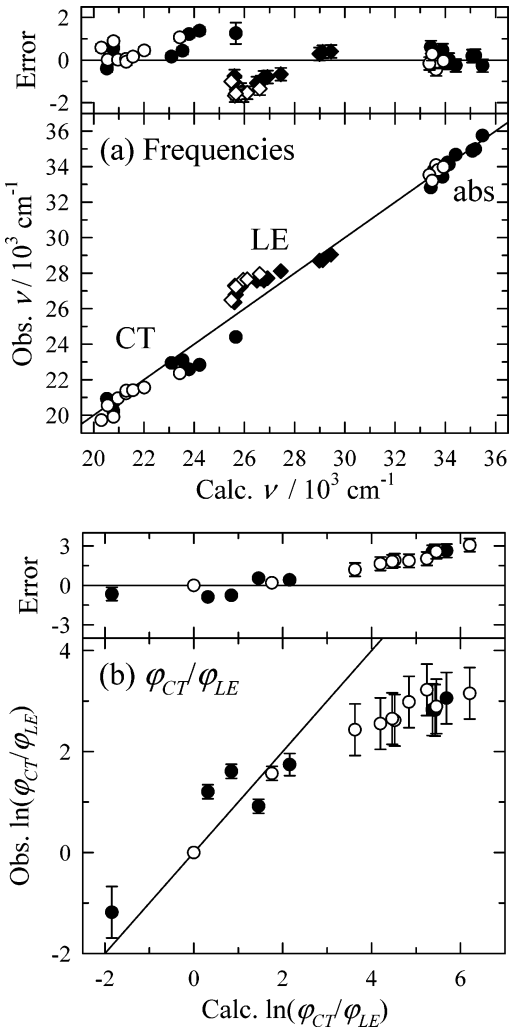

Figure 7. Results of fitting P6C data to the solvatochromic model. These results are for Fit #1(b), which involves simultaneous fit of frequency (top panel) and relative intensity (bottom panel) data with fixed values of a and α (see Table 6 and the text). Filled and open symbols denote aprotic and protic solvents, respectively.

of $\varphi_{CT}/\varphi_{LE}$. That is, fits to the frequency data imply a much greater solvent dependence of the free energy change of the CT−LE reaction (i.e., in K_{eq}) than is indicated by the CT/LE intensity ratios.

To simultaneously fit both the frequency and relative intensity data, one or more additional parameters of the model must be varied. Given the total number of parameters in the model, many possibilities exist for achieving good fits to the experimental data, but the parameter values required are unrealistic. For example, the CT/LE intensity ratio depends sensitively on the value of M_a^{CT} (really M_a^{CT}/M_b^{LE}), but to fit the data by optimizing this ratio requires very small values of M_a^{CT}, which are incompatible with the radiative rate data. The ground-state dipole moments, either μ_0 or μ_0^{CT}, can also be varied to fit the data. In this case a good fit requires values of μ_0 or μ_0^{CT} that are as much as 60% (or 4D) smaller and larger, respectively, than the MP2 predictions, differences that are far larger than the errors expected for the ab initio results. More subtle possibilities include allowing for different polarizabilities of the different states. Fit #2 in Table 6B lists the results obtained when α_a is reduced by a factor of 3 and α_0 is optimized for fixed α_b. In this case, all of the data can be simultaneously fit to approximately the same accuracy as the linear correlations shown in Figures 4 and 5. (P6C results are plotted in Figure S3.) Although the values of α_0 required are reasonable, the large differences in effective polarizabilities, $\alpha_0/\alpha_a \sim 4$, are not. Moreover, the dipole moments μ_a^{LE} are on average 61% larger than AM1/CI values, and these fits require $\mu_a^{LE} > \mu_a^{CT}$, which is in qualitative disagreement with the results of electronic structure calculations. A final parameter that can be varied is the effective cavity radius a. Results obtained when a is allowed to vary are shown as Fit #3 in Table 6B. The quality of this fit is comparable to that of Fit #2. The problem with this approach is that the cavity volumes implied by these radii are ∼40% smaller than the van der Waals volumes of the solutes, an unreasonable result. The dipole moments of the L_a state are also much smaller than predicted by electronic structure methods.

From the above observations, as well as much further experimentation,[80] it appears that there is no way to simultaneously fit both the frequency and the relative intensity data on the basis of the proposed model with meaningful parameter choices. This discrepancy implies that either our analysis is incorrect or the proposed model is oversimplified in some way. One possible source of error in the analysis concerns the assumption of rapid equilibrium, which enables the steady-state intensity ratios to be interpreted in terms of equilibrium constants (eq 6.13). As discussed in the following section, time-resolved data indicate that in some cases, mainly in protic solvents, the steady-state intensity ratios $\varphi_{CT}/\varphi_{LE}$ are smaller than limiting ($t \rightarrow \infty$) values, indicating that the steady-state spectra are not always equilibrated. This error would make the apparent equilibrium constants derived from steady-state data smaller than the true values, and cause the sort of deviations displayed in Figure 7b. Although lack of equilibration in some solvents may add to the uncertainty in the steady-state data, it does not explain the observed discrepancy. First, there is little difference in the degree of fit shown by systems where the use of steady-state data is questionable and in systems where the equilibrium assumption seems valid. In addition, as will be discussed later, time-resolved data provide an alternative means for estimating equilibrium constants, and the results obtained in this way are consistent with the estimates based on steady-state area ratios. Thus it appears that the discrepancy is probably related to some failure of the model.

We conjecture that neglect of the distribution of twist angles is likely to be the source of the difficulty. Two separate effects of the distribution may be important. First, the fact that molecules in the CT state are not confined to $\theta = 90°$ is of obvious importance by virtue of the fact that molecules precisely at $\theta = 90°$ have zero or nearly zero transition moments (Table 5, Figure 6). Thus, molecules with nonoptimal values of θ (<90°) are the ones dictating the emission characteristics.[81] The fact that the experimental values of M_{CT} are sizable probably also means that the distribution is not particularly sharp. (This "misrepresentation" of the θ distribution by the spectral intensities may also be the origin of the odd solvent insensitivity of the CT emission bandwidths.) It may be that treatment of the CT state in terms of a single effective frequency and a single effective transition moment leads to incorrect intensity predictions. A solvent-dependent difference in the widths of the LE and CT distributions could also be the source of the difficulty. These ideas will need to be tested using the full 2-dimensional model. At least for the present time, we believe that the results of Fit#1(a), which ignore the intensity data, provide sensible representations of the solution-phase energetics and dipole moments of these solutes.

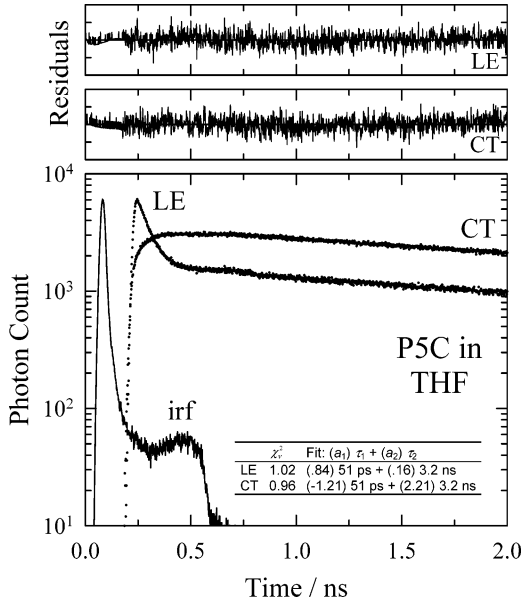

Figure 8. Representative "type 1" emission decays of P5C in tetrahydrofuran. The bottom panel shows the emission data (points) collected in the LE (352 nm) and CT (440 nm) regions. A time shifted version of the instrument response function ("irf") is also shown for comparison. The top two panels show the weighted residuals of biexponential fits to the data with linked time constants (±5 full scale). Fit parameters are listed in the inset table.

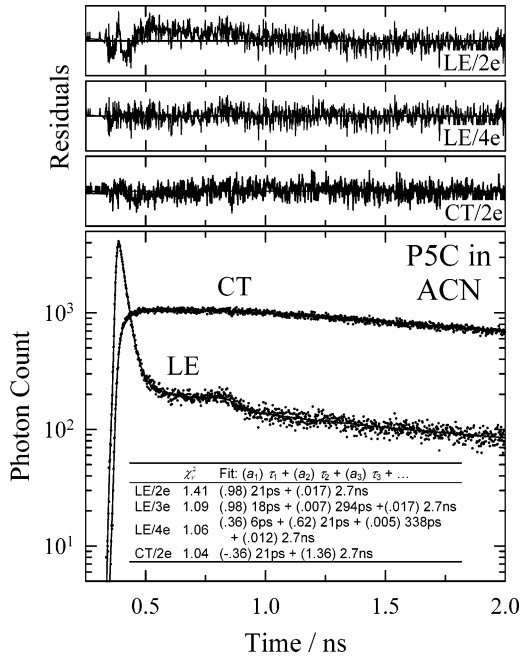

Figure 9. Representative "type 2" emission decays of P5C in acetonitrile. The bottom panel shows the emission data (points) collected in the LE (351 nm) and CT (500 nm) regions. The panel labeled "CT/2e" shows the residuals of an unconstrained two-exponential fit of the CT decay. The top two panels show the weighted residuals of constrained two-exponential ("LE/2e") and four-exponential ("LE/4e") fits to the LE decay (±5 full scale). These fits are constrained to have the same longest time constant as the CT decay. Fit parameters, including a three-exponential fit not displayed, are listed in the inset table.

VII. Dynamics

VII-A. Qualitative Behavior. We have measured time-resolved emission decays near the peaks of the LE and CT band maxima for P4C, P5C, and P6C in nearly all of the solvents listed in Table 1. In nine of these solute + solvent combinations

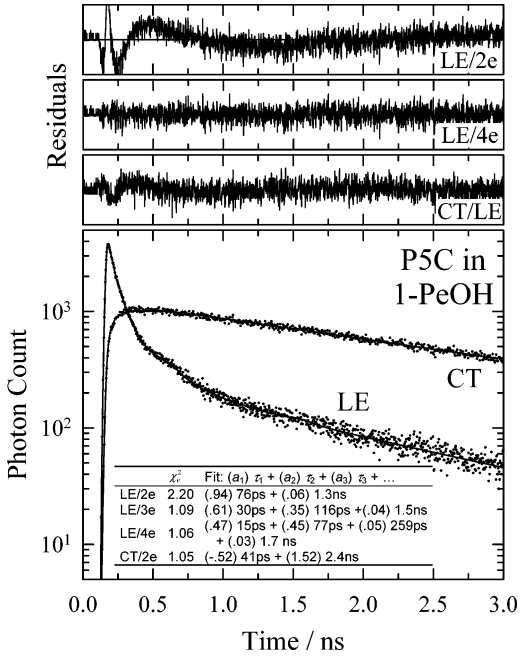

Figure 10. Representative "type 3" emission decays of P5C in 1-pentanol. The bottom panel shows the emission data (points) collected in the LE (349 nm) and CT (483 nm) emission regions. The top two panels show the weighted residuals of two-exponential ("LE/2e") and four-exponential ("LE/4e") fits to the LE decay (±5 full scale). The CT data can be described by a biexponential function (not shown but parameters provided in table inset. Using the LE decay parameters to fit the CT decay as described in the text yields the fit and residuals marked "CT/LE" with $\chi_\nu^2 = 1.09$ ($k_{LE}^{-1} = 0.24$ ns and $k_{CT}^{-1} = 3.3$ ns).

we have also derived complete time-resolved emission spectra using the spectral reconstruction method. In all cases studied, the emission kinetics appear to reflect an LE → CT interconversion, but significant departures from the classical two-state description of section III are often observed. To describe these results, we begin by surveying the LE/CT emission decays measured over the whole range of systems. Representative decays are plotted in Figures 8−10 and a summary of kinetic parameters is provided in Table 7.

As listed in Table 7 ("#" columns), we find that systems can be categorized into four groups according to the emission kinetics they exhibit. First, there is the trivial "type 0" group composed of all of the solutes in low polarity solvents for which no CT band is observed in steady-state emission. For these systems the LE band decays as a single-exponential function, indicating no observable reaction.

The simplest cases for which reaction is observed are labeled "type 1" systems. This designation indicates systems whose decay kinetics conform to the classical two-state reversible reaction mechanism described in section III. A representative example this type of behavior is shown in Figure 8, which contains data for P5C in tetrahydrofuran. In these systems, emission from the LE and CT regions can be fit to biexponential functions of time using a single pair of time constants. Systems falling into this category are P4C in all of the polar aprotic solvents studied and in many alcohols, and P5C in all but the most polar of the aprotic solvents. Rigorously biexponential decays are seldom observed in the case of P6C.

Many solute + solvent combinations exhibit kinetics that are not rigorously biexponential, but fall close to this ideal. Such systems are categorized as "type 2" systems in Table 7. They are represented by the P5C/acetonitrile example shown in Figure

TABLE 7: Summary of Fluorescence Decay Data (25 °C)

	P4C							P5C							P6C						
solvent	#	t_{eq}/ ns	τ^0_{rxn}/ ps	$\bar{\tau}_{rxn}$/ ps	τ_{dec}/ ns	$\bar{\tau}_{LE}$/ ps	ln a_{rxn}/a_{dec}	#	t_{eq}/ ns	τ^0_{rxn}/ ps	$\bar{\tau}_{rxn}$/ ps	τ_{dec}/ ns	$\bar{\tau}_{LE}$/ ps	ln a_{rxn}/a_{dec}	#	t_{eq}/ ns	τ^0_{rxn}/ ps	$\bar{\tau}_{rxn}$/ ps	τ_{dec}/ ns	$\bar{\tau}_{LE}$/ ps	ln a_{rxn}/a_{dec}
perfluorohexanes	0				1.6										0				1.2		
n-hexane	0				3.0			0				2.9			0				2.0		
methylcyclohexane								0				2.4			0				2.2		
cyclohexane	0				3.6			0				3.4			0				2.3		
benzene								1	<1	36	36	3.2		−1.3	0						
dietheyl ether	0				3.3			1	<1	63	63	2.9		−0.8	1	<1	26	26	2.3		−0.62
dichloromethane	1	>3	157	157	2.1		−0.8	2	∼1	44	85	3.1		1.9	2	<1	6	9	3.1		2.5
1,4-dioxane	1	<2	(250)	(250)	3.1			1	<1	77	77	3.1		0.6	1	<1	13	13	2.9		1.2
tetrahydrofuran	1	<2	220	220	3.2		−1.4	1	<1	52	52	3.2		1.6	2	<1	10	17	3.2		1.9
ethyl acetate	1	<2	302	302	3.0		−1.2	1	<1	58	58	3.0		1.9	2	∼1	16	23	2.9		2.0
methyl acetate	1	<1	314	314	3.0		−0.7	1	<1	48	48	2.9		2.3	2	∼1	10	16	3.0		2.4
dimethylformamide	1	∼1	215	215	2.8		2.0	2	<1	22	27	2.6		3.5							
dimethyl sulfoxide	1	∼1	160	160	2.7		0.2	2	<1	22	30	2.2		3.4	2	∼1	9	13	2.5		3.0
acetonitrile	1	∼2	258	258	2.7		2.0	2	<1	19	20	2.8		4.0	2	∼2	5	7	2.9		3.8
methanol	2	∼3	104	105	1.9	142	3.6	2	∼1	15	18	1.3	24	5.2	2	∼1	5	8	1.9	39	4.5
ethanol	2	>3	153	188	2.2	290	2.3	3	∼2	17	23	1.9	67	3.9	3	>3	11	24	2.4	78	3.9
1-propanol	2	>3	196	196	2.2	384	1.9	3	>3	31	42	2.1	64	4.2	3	>3	12	74	2.2	134	2.3
2-propanol	1/2	∼3	207	207	2.3	461	1.9	3	>3	25	43	2.3	56	4.2	3	>3	13	22	2.5	68	3.6
1-butanol	1/2	∼3	231	231	2.3	549	1.6	3	>3	37	61	2.3	85	4.1	3	∼2	26	31	2.6	72	3.5
1-pentanol	1/2	∼3	282	282	2.4	623	1.6	3	>3	45	75	2.4	117	4.1	3	∼2	23	54	2.9	192	1.9
1-decanol	1	?	329	329	1.8	789	0.6	3	>3	111	260	2.1	392	2.0	3	∼2	126	187	2.7	782	0.92
N-methylformamide								3	irr	32	64	1.6	108	4.8							
ethylene glycol	3	irr	79.2	102	1.5	121	(4)	3	irr	23	43	1.8	65	(6)	3	irr	19	34	1.6	34	(4)
formamide	3	∼3	65.9	73	1.6	82	4.0	3	irr	25	77	2.9	85	(6)	3	irr	11	50	1.7	78	(4)

[a] # indicates the type of LE decay kinetics as described in the text (0 = 1 exp; 1 = LE and CT 2 exp and same τ; 2 = LE nearly 2-exp; 3 = LE multi-exp). t_{eq} is a rough measure of the time required before emission in the LE and CT regions decay with the same logarithmic slope; "irr" denotes that equilibration is not reached before emission is too low to measure reliably. τ_{dec} denotes the longest decay time common to both the LE and CT emission. τ^0_{rxn}, $\bar{\tau}_{rxn}$, $\bar{\tau}_{LE}$, and ln(a_{rxn}/a_{dec}) are defined by eqs 7.3−7.6. Data in parentheses indicate highly uncertain values. Note that the samples used here were not deoxygenated so that the values of $\bar{\tau}_{LE}$ (especially in perfluorohexanes) may be somewhat smaller than deoxygenated values.

9. In these cases, although a biexponential representation of the decays in both the LE and CT regions provides reasonable fits to the data, three exponential components are required to fit the LE decays to within uncertainties. The LE decays are dominated by a fastest component whose time constant τ_1 matches the rise time observed in the CT region and whose fractional amplitude a_1 typically accounts for 90% or more of the decay. The LE and CT decays also possess long time constants that are equal or nearly equal, similar to the type 1 case. But in type 2 systems, if data are collected out to several lifetimes, or if the longest components of the LE and CT decays are constrained to have equal time constants, an additional small-amplitude component having an intermediate time constant becomes evident. In the P5C/acetonitrile example shown in Figure 9, a component with amplitude of less than 1% and with a time constant of ∼300 ps is required to adequately fit the data. (We use a four-exponential representation with a split fast component to provide the best representation in Figure 9, but the three-exponential fit with parameters tabulated in the inset is nearly as good.) Given that that the majority of the LE decay is contained in the fastest component, the departure from the ideal in this case, and in many others we have studied, is subtle and could be easily overlooked or disregarded. We cannot rule out the possibility that, at least in some cases, such small-amplitude intermediate components might be merely an instrumental artifact or due to some impurity in the samples. A number of checks, as well as the systematic nature of this deviation from ideal behavior in many solute + solvent combinations, suggest that these components are real, and indicative of small departures from two-state kinetics with classical time-independent rate constants. However, their presence or absence has little quantitative effect on the kinetic data presented later.

Much larger departures from classical two-state kinetics are observed in many other solute + solvent combinations, mainly in protic solvents. These "type 3" cases are characterized by LE emission that is clearly not a biexponential function of time. Here, LE decays require three or more exponential components for an adequate fit, independent of whether one tries to constrain the long time constant to match those of the CT decays. The CT decays, on the other hand, are often still reasonably represented using biexponential functions. An example of such a system, P5C in 1-pentanol, is provided in Figure 10. As illustrated by this example, we often observe that after several nanoseconds the LE and CT emission become equilibrated, i.e., decay at the same rate. Estimates of this equilibration time are listed under the headings "t_{eq}" in Table 7. In only a few cases (marked "irr" in Table 2) does it appear that the LE and CT emission decays do not equilibrate before the emission becomes too weak to observe reliably.

An initially puzzling feature of type 3 systems is that the time constants in the CT region do not match the decay times observed in the LE region. Nevertheless, the LE and CT species still bear a precursor−successor relationship to one another. This relationship can be tested if it is assumed that the complex kinetics of the LE decay result from a time-dependent rate constant for forward reaction, $k_f(t)$. As discussed at the end of section III, if k_f is the only time-dependent rate constant in the problem, the time evolution of the CT emission is completely determined by the time dependence of the LE band plus the value of the constants k_{CT} and (to a much lesser extent) k_{LE}. The panel labeled "CT/LE" in Figure 10 displays the weighted residuals of such a fit to the CT emission data. As will be discussed shortly, the slightly imperfect fit implied by the nonrandom pattern of residuals ($\chi_\nu^2 = 1.09$) can be plausibly ascribed to spectral dynamics of the CT band. Even with this

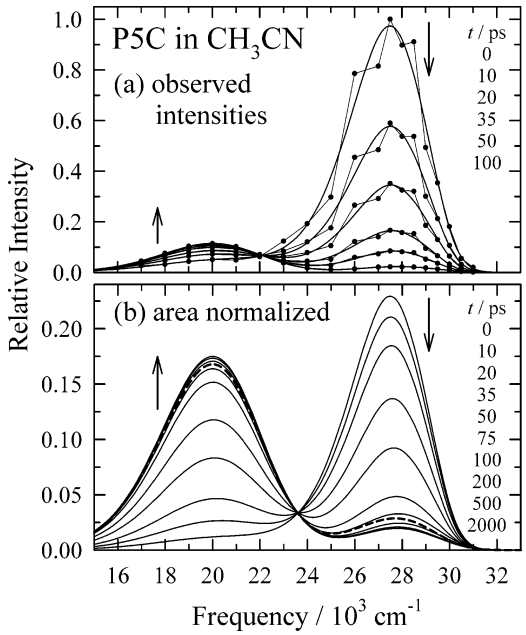

Figure 11. Time-resolved spectra of P5C in acetonitrile. (a) shows spectra with the relative intensities as recorded. The connected points are the reconstructed spectra and the smooth curves are fits to the spectra using a reference line shape as described in connection with Figure 3. (b) shows the fitted spectra normalized to have equal areas (solid lines). The heavy dashed curve is the steady-state spectrum. Arrows in both panels indicate the direction of increasing time.

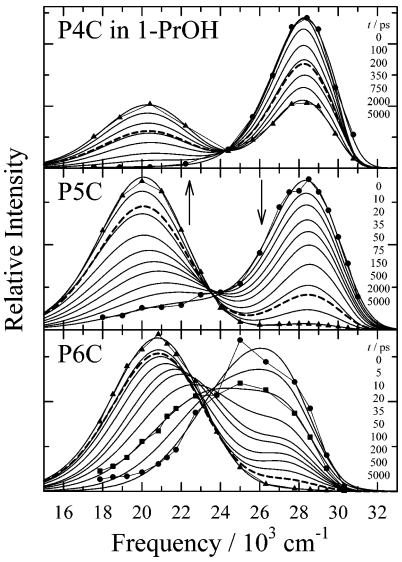

Figure 12. Area normalized spectra of P4C, P5C, and P6C in 1-propanol. Solid curves show fits to the time-resolved spectra at the times indicated. Connected points indicate the actual time-resolved data at the extreme times of 0 (circles) and 5 ns (triangles). (In the case of P6C the data at 10 ps (squares) are also displayed.) The heavy dashed lines are fits to the steady-state spectra.

flaw, the level of agreement shown in Figure 10 is sufficient to demonstrate that, despite the seemingly unrelated time constants in the LE and CT decays, the emission kinetics do indeed reflect a single LE → CT reaction. Fits of this sort made for other type 3 systems suggest that for these systems as well as for type 2 systems, complex emission kinetics in the LE region primarily result from time-dependent rates for the LE → CT reaction.

Further evidence for this assertion is found in the complete time-resolved spectra we have measured. Examples are shown in Figures 11 and 12. Figure 11 contains time-resolved spectra of P5C in acetonitrile, the type 2 system already discussed. The connected points in the top panel of Figure 11 show spectra reconstructed from a series of decays at 19 emission wavelengths. These "raw" spectra are noisy at early times because there are dynamics occurring on time scales (∼5 ps) shorter than our instrumental resolution (25 ps). However, fitting these spectra in the manner described in section IV (Figure 3) provides the smooth curves shown in this figure, which enable us to obtain accurate measurements of spectral frequencies and intensities, even at early times. In the case of P5C in acetonitrile, without constraining the decay fits in any way, we find that the LE and CT peaks maintain a constant width and position with time. The area-normalized spectra ("TRANES" spectra[82]) shown in Figure 11b display an obvious isoemissive point near 23 600 cm^{-1}, which provides clear evidence that the only process significantly affecting these spectra is the two-state LE → CT interconversion.[82,83] In the type 1 system, P5C in tetrahydrofuran (not shown) time-resolved spectra look much the same as in the P5C/acetonitrile case. The only difference is that in acetonitrile the total intensity of the LE band, like the intensity at individual wavelengths, departs slightly from a biexponential time dependence. One curious feature in the data in Figure 11 is the significant CT intensity (∼7% of the total) found in the $t = 0$ spectrum. This intensity could indicate the presence of CT product immediately upon excitation but is more likely an artifact caused by the difficulty of detecting fast (∼5 ps) rising components with the present instrumentation.

More interesting dynamics are observed in the spectra of the three P*n*C solutes in 1-propanol plotted in Figure 12. P4C in 1-propanol is a type 2 system, like P5C in acetonitrile. The kinetics are nearly biexponential. As in the latter system, we observe only small changes in the positions and widths of the LE and CT bands with time. Also similar is the presence of a clear isoemissive point in these area-normalized spectra, once again indicating a reaction between two well-defined states. Note, however, the lack of any appreciable CT intensity and the noise-free nature of the $t = 0$ spectrum in this much slower reaction ($\tau_{rxn} \sim 200$ ps) compared to the P5C/acetonitrile system ($\tau_{rxn} \sim 20$ ps). In the case of P5C in 1-propanol we no longer observe a clear isoemissive point. The spectra are still composed of two well-separated peaks whose widths do not differ greatly from the LE and CT components in the steady-state spectra. But in this case, whereas the LE band position is constant in time, the CT band shifts by ∼1500 cm^{-1} during the equilibration process. This shift spoils the chance for a distinct isoemissive point. Finally, in the case of P6C in propanol, departure from simple two-state behavior is most dramatic. At early times there is considerable overlap between the LE and CT peaks. Nevertheless, the spectra can again be fit to an LE band whose position and width do not change significantly with time and a CT band which shifts by ∼4000 cm^{-1}. The normalized time dependence of this shift is close to the solvation response function of 1-propanol measured using the coumarin 153 probe,[33] suggesting that this spectral evolution mainly reflects the solvent stabilization of the CT product. Similar observations have been previously made in the case of DMABN in propanol.[84,85] These spectral dynamics and especially the differences displayed by the three solutes in propanol are interesting and we will have more to say about them later. For the present, we mainly focus on what they suggest about measuring reaction kinetics. First, these spectra and others like them indicate that emission decays reflect LE → CT interconversion, which is sometimes accompanied by time-dependent spectral relaxation. In all cases studied, the LE band is largely time-independent in position

and width; it is the CT band which sometimes undergoes large changes with time. Monitoring the decay of the LE band at its steady-state peak should therefore provide a means of measuring the population changes resulting from reaction (and overall S_1 depopulation). Emission decays monitored near the CT maximum should largely be describable from the LE decay kinetics, but some deviations of the sort discussed with respect to Figure 10 are expected due to the spectral dynamics of the CT band.

VII-B. Effective Reaction Rates and Equilibrium Constants. With this perspective in mind, we now consider how to estimate reaction rates in such a manner that will enable comparison of all of the solute + solvent combinations examined. In type 1 cases, the determination of reaction rates is straightforward. We associate the shorter time constant (τ_1) observed in either region with the LE ↔ CT equilibration time constant τ_{rxn} and the longer time constant (τ_2) with the average population decay time τ_{dec} described in section III. These times are listed in Table 7 with $\tau_{rxn} = \tau^0_{rxn} = \bar{\tau}_{rxn}$ in the case of type 1 systems. As shown by eq 3.5, under the assumption of rapid equilibration, the ratio of the amplitudes of the fast and slow components in the LE region (if free from CT emission) provides a direct measure of the CT/LE equilibrium constant

$$K_{eq} \equiv \frac{[CT]_{eq}}{[LE]_{eq}} = \frac{a_{rxn}}{a_{dec}} \tag{7.1}$$

Values of the logarithms of these ratios are also listed in Table 7. Finally, the forward (LE → CT) reaction rate constant is given by

$$k_f = \frac{1}{\tau_{rxn}(1 + K_{eq}^{-1})} \tag{7.2}$$

In the case of type 2 and 3 systems there can be no single rate constant comparable to k_f that completely specifies the reaction kinetics. Nevertheless, effective rate "constants" can be derived by considering two limiting characteristics of the LE decay analogous to τ_{rxn} in type 1 systems.[86] Using an *n*-exponential fit of the LE emission, we assume that the component with the largest time constant ($i = n$), which is usually similar to the CT decay time, can be associated with τ_{dec} of the biexponential case. Excluding this time constant (except in the case of irreversible reactions) we define the initial reaction time

$$\tau^0_{rxn} = \frac{\sum_{i=1}^{n-1} a_i}{\sum_{i=1}^{n-1} (a_i/\tau_i)} \tag{7.3}$$

and the average reaction time

$$\bar{\tau}_{rxn} = \frac{\sum_{i=1}^{n-1} a_i\tau_i}{\sum_{i=1}^{n-1} a_i} \tag{7.4}$$

where a_i and τ_i are the fractional amplitudes and time constants observed in *n*-exponential fits. The three quantities τ^0_{rxn}, $\bar{\tau}_{rxn}$, and $\tau_{dec} \sim \tau_n$ are listed in Table 7. Also provided are the average LE decay times,

$$\bar{\tau}_{LE} = \sum_{i=1}^{n} a_i\tau_i \tag{7.5}$$

which are used in place of $\bar{\tau}_{rxn}$ in the case of irreversible reactions, and the amplitude ratios

$$\text{“}(a_{rxn}/a_{dec})\text{”} = \sum_{i=1}^{n-1} a_i/a_n \tag{7.6}$$

(The latter ratio is only meaningful for reversible reactions.)

Examination of Table 7 shows that in type 2 systems the two measures of reaction time defined above differ by only a modest amount. $\bar{\tau}_{rxn}$ is on average ~35% larger than τ^0_{rxn} in type 2 systems, reflecting the modest departure from biexponential kinetics observed in these cases. In type 3 systems, the departure is greater and $\bar{\tau}_{rxn}$ averages twice τ^0_{rxn}. But, whichever of these two measures is chosen for the reaction time, there is a clear separation between τ_{rxn} and the longest time constant observed, τ_{dec}, with average values of τ_{dec}/τ_{rxn} being more than 10, 50, and 100 for P4C, P5C, and P6C, respectively. This observation supports the assumption of rapid equilibration, required to interpret the fast and slow times in the emission decays as being due to separable reaction and population decay rates (section III). However, especially in type 3 systems, small-amplitude components with time constants much larger than $\bar{\tau}_{rxn}$, in some cases as large as 1 ns, are present. (One example is provided by the P5C in pentanol data in Figure 10, where the long time constants of the LE and CT decays differ even out to 3 ns.) The effect of these small-amplitude slow components on the steady-state spectra can be significant, as illustrated by the data in Figures 11 and 12. In the case of P5C in acetonitrile (Figure 11) the long-time ratio of CT/LE band intensities is reasonably close to what is observed in the steady-state spectra (heavy dashed curves), but in the 1-propanol examples of Figure 12, the deviation is more significant. In terms of ratios ($\varphi_{CT}/\varphi_{LE}$) analyzed in section VI, we find that the steady-state values can be smaller than the long-time values by as much a factor of 5−10 in extreme cases. Beyond the errors produced in using the steady-state ratios, it is not clear how these slow components might alter the interpretation of the times. We leave such questions to later work. For purposes of the present survey, we simply assume that τ^0_{rxn} and $\bar{\tau}_{rxn}$ provide useful bounds on a quantity that is equivalent to τ_{rxn} measured in type 1 systems. We also assume that the amplitude ratios defined by eq 7.6 can be used in eq 7.1 to obtain estimates of the equilibrium constants for reaction, except, of course, where the reaction appears to be irreversible.

We first consider the equilibrium constants. To obtain the best estimates of the equilibrium constants for reaction, we compared the values deduced from the amplitude ratios in Table 7, $K^a_{eq} = (a_{rxn}/a_{dec})$, with the steady-state quantities $K^{\varphi} \equiv (\varphi_{CT}\nu_{LE}^3)/(\varphi_{LE}\nu_{CT}^3)$. (These data are plotted in Figure S4 of the Supporting Information.) Assuming solvent independence of the transition moments and equilibrated emission, the latter ratio should be related to K_{eq} by $K^{\varphi}_{eq} = K_{eq}(M_{CT}^2/M_{LE}^2)$. In P4C and P5C the correlation between K^a_{eq} and K^{φ} is quite good, with the few outlying points observed being associated with solvents where interpretation of the time-resolved amplitudes is most uncertain. In contrast, in the case of P6C the correlation is poor unless most of the data from the protic solvents is excluded. Excluding the outlying (P4C and P5C) or protic (P6C)

TABLE 8: Summary of LE → CT Reaction Parameters (25 °C)[a]

	P4C		P5C		P6C	
solvent	Δ_rG/kJ mol^{-1}	$k_f/10^{10}$ s^{-1}	Δ_rG/kJ mol^{-1}	$k_f/10^{10}$ s^{-1}	Δ_rG/kJ mol^{-1}	$k_f/10^{10}$ s^{-1}
benzene			3.1 ± 0.6	0.62 ± 0.46		
diethyl ether			1.9 ± 0.6	0.50 ± 0.26	1.5 ± 0.6	1.4 ± 0.8
dichloromethane	1.9 ± 0.6	0.20 ± 0.14	−4.9 ± 0.5	1.4 ± 0.4	−6.2 ± 0.5	12 ± 7
1,4-dioxane			−1.7 ± 0.3	0.86 ± 0.15	−2.5 ± 0.4	5.5 ± 1.4
tetrahydrofuran	3.6 ± 0.5	0.09 ± 0.06	−3.9 ± 0.3	1.6 ± 0.2	−4.4 ± 0.4	6.3 ± 1.6
ethyl acetate	2.8 ± 0.5	0.08 ± 0.05	−4.7 ± 0.3	1.5 ± 0.2	−4.9 ± 0.3	4.5 ± 1.3
methyl acetate	1.7 ± 0.5	0.11 ± 0.04	−5.6 ± 0.3	1.9 ± 0.2	−6.0 ± 0.3	7.0 ± 2.6
dimethylformamide	−5.1 ± 0.4	0.41 ± 0.02	−9.6 ± 0.5	4.0 ± 0.7		
dimethyl sulfoxide	−5.9 ± 0.4	0.57 ± 0.03	−9.7 ± 0.6	3.7 ± 0.7	−9.4 ± 1.1	9.2 ± 2.6
acetonitrile	−4.8 ± 0.4	0.34 ± 0.02	−10.0 ± 0.6	5.1 ± 0.8	−9.4 ± 0.4	16 ± 7
methanol	−7.9 ± 0.3	0.92 ± 0.09	−11.8 ± 0.7	6.2 ± 0.7	−10.7 ± 1.2	16 ± 5
ethanol	−6.1 ± 0.4	0.54 ± 0.19	−9.7 ± 0.8	4.8 ± 0.7	(−10)	5.7 ± 3.3
1-propanol	−5.2 ± 0.4	0.45 ± 0.11	−9.7 ± 0.6	2.7 ± 1.8	(−7)	2.2 ± 1.6
2-propanol	−4.9 ± 0.3	0.43 ± 0.05	−9.3 ± 1.0	2.9 ± 1.6	(−9)	5.5 ± 3.1
1-butanol	−4.4 ± 0.4	0.37 ± 0.04	−9.0 ± 1.0	2.0 ± 0.6	−8.7 ± 1.0	3.4 ± 0.9
1-pentanol	−3.9 ± 0.4	0.29 ± 0.03	−8.8 ± 1.0	1.6 ± 0.5	−7.5 ± 1.1	2.5 ± 1.3
1-decanol	−1.2 ± 0.6	0.19 ± 0.04	−4.7 ± 0.4	0.5 ± 0.2	−4.1 ± 0.9	0.54 ± 0.17
N-methylformamide			(−10)	1.4 ± 0.8		
ethylene glycol	(−4)	0.83 ± 0.21	(−8)	2.2 ± 1.0	(−10)	3.7 ± 2.8
formamide	−7.3 ± 0.4	1.3 ± 0.3	(−9)	1.8 ± 1.6	(−10)	2.2 ± 1.6

[a] Values of Δ_rG in parentheses indicate that the reaction appeared to be irreversible on the emission time scale so that the values listed should be considered upper limits. Values listed under the headings k_f are "best estimates" of effective forward reaction rate constants in the case of type 2 and 3 systems. In these cases k_f is determined from the average of τ^0_{rxn} and $\bar{\tau}_{rxn}$ (or τ^0_{rxn} and $\bar{\tau}_{LE}$ in systems thought to be irreversible), and the "uncertainties" are the larger of $^1/_2$ the difference between the two values and the estimated uncertainty in $\bar{\tau}_{rxn}$.

data points, these correlations yielded estimates of the ratios M_{CT}/M_{LE} of 0.38 ± 0.05 (P4C), 0.57 ± 0.05 (P5C), and 0.90 ± 0.06 (P6C). The fact that these values are within uncertainties of the average values deduced from the quantum yield measurements (Table 4), 0.4 ± 0.1 (P4C), 0.7 ± 0.1 (P5C), and 0.9 ± 0.1 (P6C), provides confidence in the consistency of this approach. Final estimates of K_{eq} were determined from weighted averages of K^a_{eq} and K^{φ}_{eq} using the average values of M_{CT}/M_{LE}.

Values of K_{eq} are presented in the form of reaction free energies, $\Delta_rG = -RT \ln K_{eq}$, in Table 8, and plotted versus the dielectric factor $d_c(\epsilon)$ in Figure 13. The free energies determined here are in good agreement with the few values available from prior measurements in acetonitrile:[19] Δ_rG(P4C) ∼ −4 kJ/mol and Δ_rG(P5C) ∼ −12 kJ/mol. In general, the driving force ($-\Delta_rG$) for reaction in a given solvent is significantly smaller for P4C than for P5C and P6C. The latter solutes display comparable values of Δ_rG in all solvents. On average, Δ_rG for the reaction of P4C is 4.5 kJ/mol less negative than for the P5C reaction, which is in turn only about 0.7 kJ/mol less negative than the P6C reaction. The reaction free energies are reasonably correlated with dielectric continuum models, as illustrated in Figure 13. We note that, as a result of the close correspondence between K^a_{eq} and K^{φ}_{eq}, these correlations differ only slightly from the steady-state results of Figure 5. These correlations show that the LE → CT reaction is unfavorable by ∼7 (P5C, P6C) and ∼18 kJ/mol (P4C) in a nonpolar solvent like cyclohexane and favorable by 6−10 kJ/mol in a highly polar solvent such as acetonitrile (at 25 °C). The fact that equilibrium between the LE and CT forms can be observed over a wide range of solvents is a result of the relatively modest change of only 7−10 k_BT in Δ_rG with solvent, coupled to the fortunate occurrence of $\Delta_rG = 0$ at dielectric constants of between 5 and 8 in all three solutes.

Effective rate constants k_f derived from K_{eq} and τ_{rxn} (eq 7−2) are also listed in Table 8. In type 2 and 3 systems, the value of k_f listed is the average of the values computed using τ^0_{rxn} and $\bar{\tau}_{rxn}$ in eq 7−2. The uncertainty is either $^1/_2$ of the difference between these two values or the estimated uncertainty in $\bar{\tau}_{rxn}$, whichever is larger. Again, there is good agreement between

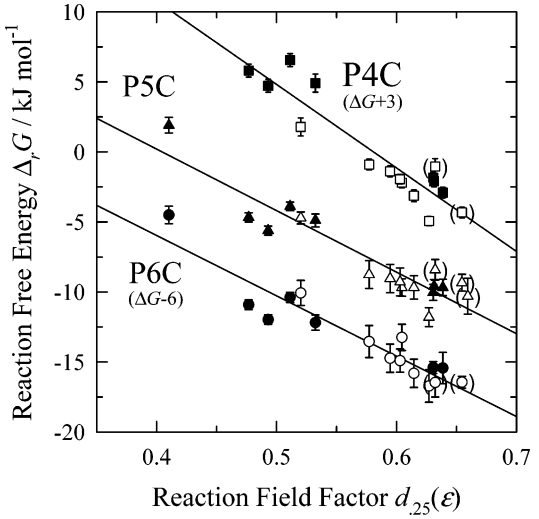

Figure 13. Reaction free energies Δ_rG versus the dielectric factor $d_c(\epsilon)$ ($c = 0.25$). Solid and open symbols denote aprotic and protic solvents, respectively. Points in parentheses are systems believed to exhibit irreversible kinetics (Δ_rG values highly uncertain). The P4C and P6C data have been vertically shifted by +3 and −6 kJ/mol for clarity. Data in benzene and dioxane have been omitted from the correlation. The linear regressions shown here are as follows. P4C(squares): Δ_rG/kJ mol^{-1} = 32.4−60.7$d_{0.25}(\epsilon)$ ($N = 16$, $\sigma = 1.3$) P5C(triangles): Δ_rG/kJ mol^{-1} = 17.2−42.3$d_{0.25}(\epsilon)$ ($N = 18$, $\sigma = 1.0$) P6C(circles): Δ_rG/kJ mol^{-1} = 17.4−43.9$d_{0.25}(\epsilon)$ ($N = 16$, $\sigma = 1.0$) where N is the number of data points and σ the standard error of the fit.

the values determined here and those reported by Zachariasse and co-workers[19] in acetonitrile: k_f(P4C) ∼ 0.3 × 10^{10} s^{-1}, k_f(P5C) ∼ 6 × 10^{10} s^{-1}, and τ_{rxn}(P6C) ∼ 6 ps. In a given solvent, the variations in reaction rate with solute generally mirror the variations in Δ_rG. Thus, on average the rates of P4C are ∼10-fold smaller than those of P5C, and those of P5C are only approximately 2-fold slower than those of P6C. Especially in the cases of P5C and P6C, these reactions are all quite rapid, and it is useful to consider what their rates imply about the possible magnitudes of barriers to reaction, ΔG^*. If one adopts

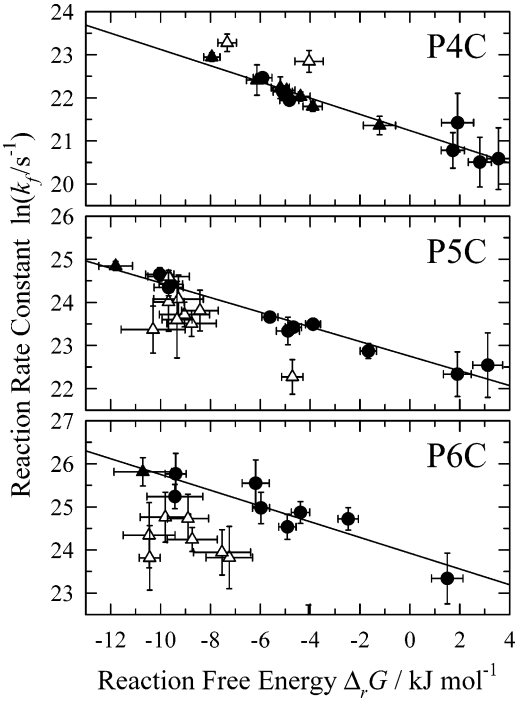

Figure 14. Rate constants k_f versus the free energy changes $\Delta_r G$ of the LE → CT reaction. Circles denote polar aprotic solvents and triangles protic solvents. Open symbols denote type 3 solvents, which are not included in the linear regressions plotted.

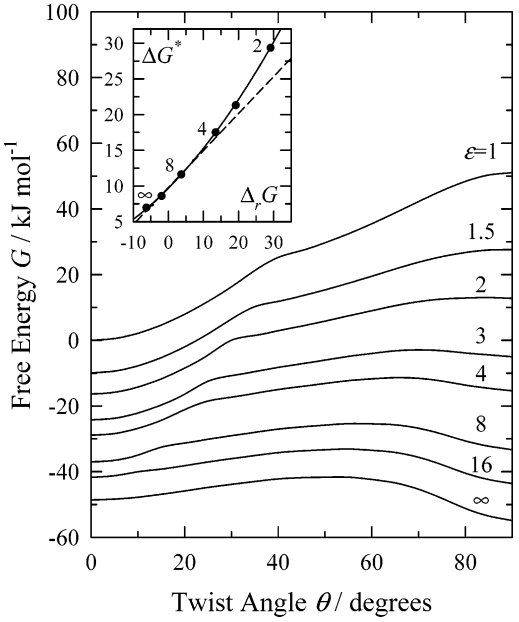

Figure 15. Calculated solution-phase potentials of P5C as a function of solvent dielectric constant. These results were obtained using the AM1/CI electronic structure method coupled to the COSMO reaction field approach.[92] The inset shows the relationship between the barrier heights ΔG^* and free energy change $\Delta_r G$ of these potentials. The curve shown here is a quadratic fit of all of the data and the dashed line is a fit of the data in the region $5 < \epsilon < \infty$.

a Kramer's type model for the barrier crossing[87,88] the rate can be expressed

$$k_f = \kappa \nu_R \exp(-\Delta G^*/k_B T) \tag{7.7}$$

where ν_R is the reactant well frequency and κ the frictional transmission coefficient ($\kappa \leq 1$). Using a value of $\nu_R \sim 2 \times 10^{12}$ s^{-1} ($\sim$75 cm^{-1})[89] and ignoring solvent friction ($\kappa = 1$), typical values of k_f in Table 8 imply barrier heights of $\sim 6\ k_B T$ (16 kJ/mol) for P4C and $3-4\ k_B T$ (10 kJ/mol) for the P5C and P6C reactions. Given that even smaller ("intrinsic"[90]) barriers would be calculated in the presence of friction ($\kappa < 1$), it is clear that these reactions are, if not truly barrierless, at least close to the limit where conventional (i.e., high-barrier) kinetics might break down. Thus, it is reasonable that many of the P5C and P6C systems exhibit signs of nonexponential reaction kinetics.

A clear correlation exists between the rate and driving force for reaction in these systems, as illustrated in Figure 14. In all three solutes, if attention is limited to type 1 and type 2 systems (filled symbols), a quantitative connection is apparent between k_f and $\Delta_r G$. Correlations such as those in Figure 14 are most often interpreted as indicating a relationship of the form $\delta\Delta G^* \approx \alpha\delta(\Delta_r G)$, wherein changes in the barrier to reaction, ΔG^*, and net energetics, $\Delta_r G$, are connected by small variation ("δ") in some control parameter, in this case solvent polarity. There are many ways to rationalize this sort of relationship and the meaning of the proportionality constant (or "Brönsted coefficient") α.[91] In the present context it is perhaps most instructive to note that just such a relationship is predicted by model calculations on the P*n*C reactions. An example is provided in Figure 15, where we plot the solution-phase S_1 potentials of P5C calculated using a self-consistent reaction field AM1/CI method.[92] As a function of solvent dielectric constant, the $\theta = 0 \rightarrow \theta = 90°$ transition goes from being too endergonic to occur in the gas phase ($\epsilon = 1$) to being $\sim$8 kJ/mol exergonic at the $\epsilon \rightarrow \infty$ limit. (Note the semiquantitative agreement of these values with the experimentally determined values of $\Delta_r G$ described above.) The dependence of the predicted barrier height with $\Delta_r G$ as ϵ is varied is plotted on the inset to Figure 15. The dashed line shows that over the interval relevant to experiment ($5 < \epsilon < \infty$) ΔG^* is an approximately linear function of $\Delta_r G$ with a slope of $\alpha = 0.52$. For comparison, the slopes of the correlation lines in Figure 14 yield empirical α values of 0.47 (P4C), 0.42 (P5C), and 0.45 (P6C). We consider this correspondence between the experimental data and the model calculations to be good evidence that the solvent dependence of the observed reaction rates in type 1 and type 2 systems is largely governed by variations in nonnegligible barriers to reaction.

Some indication of the relevance of solvent friction for determining the rates of these reactions can be gleaned by examining the "residual rate constant" defined by

$$\kappa_{res} \equiv k_f/k_{fit}(\Delta_r G) \tag{7.8}$$

where $k_{fit}(\Delta_r G)$ denotes the rate predicted for a given driving force by the empirical correlations in Figure 14. The quantity κ_{res} is not directly the transmission factor (κ) of the Kramer's model, but, to the extent that the correlations in Figure 14 capture the solvent dependence of ΔG^* (i.e., the static solvent effect on the rate) this quantity should be proportional to κ and serve to display the solvent dependence of the transmission coefficient. In Figure 16 such residual rate constants are plotted versus one measure of solvent friction, dipolar solvation times measured with the coumarin 153 probe, $\langle\tau_{C153}\rangle$.[34,33] Quite similar plots are obtained using bulk viscosity as the measure of solvent friction (Figure S5 of the Supporting Information). Figure 16 suggests that, at least in the case of P5C and P6C, the different behavior of the type 3 systems in the $k_f - \Delta_r G$ correlations of Figure 14 is due to the influence of solvent friction. The type 3 systems all involve protic solvents which solvate much more slowly and are more viscous than the solvents in type 1 and 2

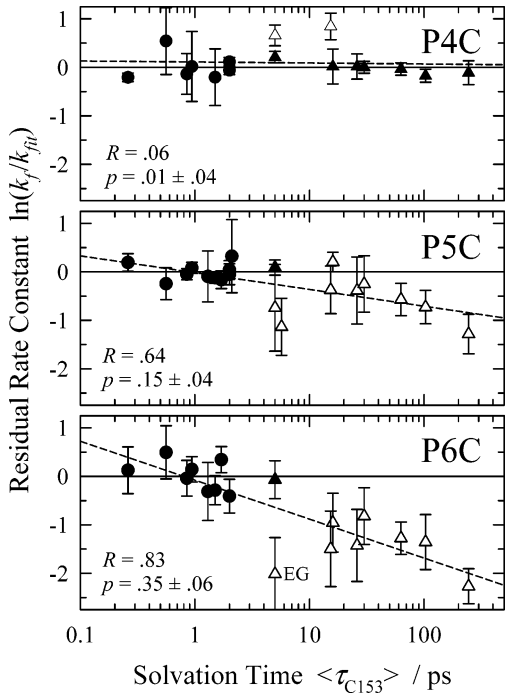

Figure 16. "Residual rate constants" κ_{res} (eq 7−4) versus integral solvation times of coumarin 153 $\langle\tau_{C153}\rangle$.[34,33] Circles denote aprotic and triangles protic solvents. Open symbols denote type 3 systems. The dashed lines are fits to all of the data. *R* is the correlation coefficient of the fit and *p* the power in the relationship $\kappa_{res} \propto \langle\tau_{C153}\rangle^{-p}$. (A listing of solvation times used here is provided in Table S4 of the Supporting Information.)

systems. If the LE → CT reaction in P6C was controlled by the same solvent friction as solvation of the dipolar probe coumarin 153, in the Smoluchowski limit of Kramer's theory[87,88] one would expect $\kappa_{res} \propto \langle\tau_{C153}\rangle^{-1}$. The linear regressions shown in Figure 16 indicate much weaker dependence, $\kappa_{res} \propto \langle\tau_{C153}\rangle^{-p}$ with the maximum value of $p = 0.35$ in the case of P6C. Alternatively, using viscosity as a measure of the friction, where the expectation is $\kappa_{res} \propto \eta^{-p}$, with $p = 1$, the P6C data yield $p = 0.56 \pm 0.10$, and the P5C data $p = 0.25 \pm 0.07$. Thus, with either choice of friction representation, the dependence of the rate on solvent friction is weaker than might be anticipated for full frictional control. Unfortunately, there is no distinction between the quality of the correlations of κ_{res} with $\langle\tau_{C153}\rangle$ compared to η, so the present data provide no hint as to whether solvent friction acts mainly via coupling to the charge transfer, to the twisting motion, or both.

VIII. Summary and Conclusions

In this paper we have examined the LE → CT reactions of three members of the "P*n*C" series of aminobenzonitrile solutes in a wide range of solvents using both steady-state and time-resolved emission spectroscopy. Our ultimate goal is to learn how to model the solution-phase reaction potentials of these solutes to understand more fully how charge transfer is controlled by static and dynamic solvent effects. As a first step toward this goal, we have surveyed the solvent dependence of the steady-state spectra of these molecules and attempted to fit the main characteristics of the spectra to a simplified version of a 2-dimensional model of the solution-phase surfaces. The model we employ is similar to models previously described for related systems by several groups.[38−47] The main new feature of the present work is the attempt to directly fit such a model to experimental data, with some guidance from electronic structure calculations. We find that a dielectric continuum treatment describes the solvent dependence of the spectral frequencies with reasonable accuracy and provides state-specific dipole moments and energies in satisfying agreement with semiempirical calculations. The results suggest that P4C, P5C, P6C, and to a lesser extent ABN, possess similar electronic properties. The differences these solutes display in their LE → CT reactions appear to mainly reflect modulation of the gas-phase LE − CT energy difference by the size of the amino alkyl ring. An important failure of the present modeling is that it is not possible to simultaneously fit the frequency data together with the observed CT/LE intensity ratios using sensible model parameters. We conjecture that this shortcoming is due to the neglect of the distribution over torsional angles, and we are currently investigating a more complete version of the model to test this idea.

The reactions studied here display a range of behaviors as a function of solute and solvent. The emission kinetics observed primarily reflect the LE → CT reaction, with some effects of spectral relaxation of the CT band also evident in some cases. In fewer than half of the solute + solvent combinations examined is classical two-state kinetic behavior observed. Most systems show some departure from biexponential decay kinetics, which can be interpreted in terms of time-dependent rate constants for the forward reaction. The occurrence of this nonclassical behavior is sensibly correlated to estimated barriers to reaction and to the frictional properties of the solvents involved. In P4C, where reaction is the slowest ($\tau_{rxn} \sim 200$ ps), classical or nearly classical kinetics are observed in most solvents. In P5C and especially P6C, where reaction is faster (τ_{rxn}(P5C) < 50 ps, τ_{rxn}(P6C) < 20 ps in most solvents), much more complicated decays of LE emission are observed. Similar complex kinetics have been observed previously,[9,14,16,17] mainly for DMABN in low-temperature alcohols.[25−28] Such behavior has most often been interpreted in terms of various models for irreversible, barrierless reaction. The present work suggests a different picture. Correlations between the rates and driving force for reaction suggest that small (3−4 k_BT) barriers are present in P5C and P6C in most solvents. The residual rates obtained after crudely accounting for the polarity dependence of these barriers are correlated to measures of solvent friction. Both polar solvation times and solvent viscosity correlate the data equally well, and it is therefore not possible to discern whether the frictional effect is primarily "dielectric" or "mechanical" or some combination of the two. But the fact that only those systems for which large departures from simple kinetic behavior are observed are ones where the effect of solvent friction is found to be important leaves little doubt as to the origins of the nonclassical behavior.

We note that in the collection of solvents studied here, only protic solvents, primarily normal alcohols, clearly exhibit the effects of solvent friction. Although differential hydrogen bonding to the LE and CT states has recently been suggested to be the source of complex emission kinetics in DMABN,[93] we do not believe that such effects are primary. We observe nonclassical kinetics in aprotic solvents as well. The fact that the frictional effects cause only modest departures from bi-exponential decay kinetics in the aprotic solvents studied here (but see ref 16) merely reflects the much lower friction in these solvents. Finally, we note that modeling the frictional effects of solvent on these reactions using irreversible reaction models may be inappropriate. In at least some cases, spectral evolution of the product CT emission is observed on the same time scales as the LE decay and it may be that equilibration of the product

state is rate limiting despite the fact that the final equilibrium heavily favors product. Hopefully, more time-resolved spectra of this sort, as well as detailed modeling using 2-dimensional surfaces, both currently in progress, will test this conjecture and lead to a better appreciation for the role that solvent friction plays in these interesting reactions.

Acknowledgment. We thank Klaas Zachariasse and Wolfang Rettig for helpful discussions concerning these reactions, Ms. Hui Jin and Dr. Hongping Li for making several of the measurements reported here, and the Office of Basic Energy Sciences of the U.S. Department of Energy for sponsoring this work.

Supporting Information Available: Tables of steady-state spectral characteristics, solvent properties, and spectral characteristics correlated with $d_c(\epsilon)$ and figures giving absorption and emission spectra, data fitting, intensity ratios, and residual rate constants. This material is available free of charge via the Internet at http://pubs.acs.org.

References and Notes

(1) Grabowski, Z. R.; Rotkiewicz, K.; Rettig, W. *Chem. Rev.* **2003**, *103*, 3899.
(2) Lippert, E.; Rettig, W.; Bonačić-Koutecký, V.; Heisel, F.; Miehé, J. A. *Adv. Chem. Phys.* **1987**, *68*, 1.
(3) Grabowski, Z. R.; Rotkiewicz, K.; Siemiarczuk, A.; Cowley, D. J.; Baumann, W. *Nouv. J. Chim.* **1979**, *3*, 443.
(4) Zachariasse, K. A.; Druzhinin, S. I.; Bosch, W.; Machinek, R. *J. Am. Chem. Soc.* **2004**, *126*, 1705.
(5) Techert, S.; Zachariasse, K. A. *J. Am. Chem. Soc.* **2004**, *126*, 5593.
(6) Zachariasse, K. A. *Chem. Phys. Lett.* **2000**, *320*, 8.
(7) See also the recent proposal of an intermediate in: Zgierski, M. Z.; Lim, E. C. *Chem. Phys. Lett.* **2004**, *393*, 143.
(8) Rettig, W. *J. Luminesc.* **1980**, *26*, 21.
(9) Rettig, W. *J. Phys. Chem.* **1982**, *86*, 1970.
(10) Rettig, W.; Gleiter, R. *J. Phys. Chem.* **1985**, *89*, 4674.
(11) Rettig, W.; Wermuth, G. *J. Photochem.* **1985**, *28*, 351.
(12) Al-Hassan, K. A.; Rettig, W. *Chem. Phys. Lett.* **1986**, *126*, 273.
(13) LaFemina, J. P.; Duke, C. B.; Rettig, W. *Chem. Phys.* **1990**, *87*, 2151.
(14) Rettig, W. *Ber. Bunsen-Ges. Phys. Chem.* **1991**, *95*, 259.
(15) Baumann, W.; Bischof, H.; Frohling, J.-C.; Brittinger, C. *J. Photochem. Photobiol. A* **1992**, *64*, 49.
(16) Braun, D.; Rettig, W. *Chem. Phys.* **1994**, *180*, 231.
(17) Braun, D.; Rettig, W. *Chem. Phys. Lett.* **1997**, *268*, 110.
(18) Yatsuhashi, T.; Trushin, S. A.; Fuss, W.; Rettig, W.; Schmid, W. E.; Zilberg, S. *Chem. Phys.* **2004**, *296*, 1.
(19) Zachariasse, K. A.; Grobys, M.; von der Haar, T.; Hebecker, A.; Il'ichev, Y. V.; Jiang, Y.-B.; Morawski, O.; Kühnle, W. *J. Photochem. Photobiol. A* **1996**, *102*, 59.
(20) von der Haar, T.; Hebecker, A.; Il'ichev, Y.; Jiang, Y.-B.; Kühnle, W.; Zachariasse, K. A. *Rec. Trav. Chim. Pays-Bas* **1995**, *114*, 430.
(21) Zachariasse, K. A.; von der Haar, T.; Leinhos, U.; Kühnle, W. *J. Inf. Rec. Mater.* **1994**, *21*, 501.
(22) Rettig, W.; Zietz, B. *Chem. Phys. Lett.* **2000**, *317*, 187.
(23) W. Song and M. Maroncelli, unpublished results.
(24) Parusel, A. B. J. *Chem. Phys. Lett.* **2001**, *340*, 531.
(25) Heisel, F.; Miehé, J. A. *Chem. Phys. Lett.* **1983**, *100*, 183.
(26) Heisel, F.; Miehé, J. A. *Chem. Phys.* **1985**, *98*, 233.
(27) Heisel, F.; Miehé, J. A.; Martinho, J. M. G. *Chem. Phys.* **1985**, *98*, 243.
(28) Su, S.-G.; Simon, J. D. *J. Chem. Phys.* **1988**, *89*, 908.
(29) Stratt, R. M.; Maroncelli, M. *J. Phys. Chem.* **1996**, *100*, 12981.
(30) Maroncelli, M. *J. Mol. Liq.* **1993**, *57*, 1.
(31) Barbara, P. F.; Jarzeba, W. *Adv. Photochem.* **1990**, *15*, 1.
(32) Hynes, J. T. Charge-Transfer Reactions and Solvation Dynamics. In *Ultrafast Dynamics of Chemical Systems*; Simon, J. D., Ed.; Kluwer: Dordrecht, 1994; p 345.
(33) Horng, M. L.; Gardecki, J. A.; Papazyan, A.; Maroncelli, M. *J. Phys. Chem.* **1995**, *99*, 17311.
(34) Reynolds, L.; Gardecki, J. A.; Frankland, S. J. V.; Horng, M. L.; Maroncelli, M. *J. Phys. Chem.* **1996**, *100*, 10337.
(35) Sumi, H.; Marcus, R. A. *J. Chem. Phys.* **1986**, *84*, 4894.
(36) Nadler, W.; Marcus, R. A. *J. Chem. Phys.* **1987**, *86*, 3906.
(37) Simon, J. D.; Doolen, R. *J. Am. Chem. Soc.* **1992**, *114*, 4861.
(38) Moro, G. J.; Nordio, P. L.; Polimeno, A. *Mol. Phys.* **1989**, *68*, 1131.
(39) Polimeno, A.; Barbon, A.; Nordio, P. L.; Rettig, W. *J. Phys. Chem.* **1994**, *98*, 12158.
(40) Nordio, P. L.; Polimeno, A.; Saielli, G. *J. Photochem. Photobiol. A* **1997**, *105*, 269.
(41) Nordio, P. L.; Polimeno, A. *Mol. Phys.* **1996**, *88*, 315.
(42) Braun, D.; Nordio, P.; Polimeno, A.; Saielli, G. *Chem. Phys.* **1996**, *208*, 127.
(43) Fonseca, T.; Kim, H. J.; Hynes, J. T. *J. Mol. Liq.* **1994**, 161.
(44) Fonseca, T.; Kim, H. J.; Hynes, J. T. *J. Photochem. Photobiol. A* **1994**, *82*, 67.
(45) Kim, H. J.; Hynes, J. T. *J. Photochem. Photobiol. A* **1997**, *105*, 337.
(46) Gedeck, P.; Schneider, S. *J. Photochem. Photobiol. A* **1997**, *105*, 165.
(47) Gedeck, P.; Schneider, S. *J. Photochem. Photobiol. A* **1999**, *121*, 7.
(48) Velapoldi, R.; Mielenz, K. *A Fluorescence Standard Reference Material:" Quinine Sulfate Dihydrate*; National Bureau of Standards: Washington, DC, 1980; Vol. Special Publications 260-64.
(49) Heitz, M. P.; Maroncelli, M. *J. Phys. Chem. A* **1997**, *101*, 5852.
(50) Frisch, M. J.; Trucks, G. W.; Schlegel, H. B.; Scuseria, G. E.; Robb, M. A.; Cheeseman, J. R.; Zakrzewski, V. G.; Montgomery, J. A., Jr.; Stratmann, R. E.; Burant, J. C.; Dapprich, S.; Millam, J. M.; Daniels, A. D.; Kudin, K. N.; Strain, M. C.; Farkas, O.; Tomasi, J.; Barone, V.; Cossi, M.; Cammi, R.; Mennucci, B.; Pomelli, C.; Adamo, C.; Clifford, S.; Ochterski, J.; Petersson, G. A.; Ayala, P. Y.; Cui, Q.; Morokuma, K.; Rega, N.; Salvador, P.; Dannenberg, J. J.; Malick, D. K.; Rabuck, A. D.; Raghavachari, K.; Foresman, J. B.; Cioslowski, J.; Ortiz, J. V.; Baboul, A. G.; Stefanov, B. B.; Liu, G.; Liashenko, A.; Piskorz, P.; Komaromi, I.; Gomperts, R.; Martin, R. L.; Fox, D. J.; Keith, T.; Al-Laham, M. A.; Peng, C. Y.; Nanayakkara, A.; Challacombe, M.; Gill, P. M. W.; Johnson, B.; Chen, W.; Wong, M. W.; Andres, J. L.; Gonzalez, C.; Head-Gordon, M.; Replogle, E. S.; Pople, J. A. *Gaussian 98*, revision A.11.3; Gaussian, Inc.: Pittsburgh, PA, 2002.
(51) AMPAC. 6.55 ed.; Semichem Inc.: 7128 Summit, Shawnee, KS 66216, 1999.
(52) Klampt, A. *J. Phys. Chem.* **1995**, *99*, 2224.
(53) Cramer, C. J.; Truhlar, D. G. *Chem. Rev.* **1999**, *99*, 2161.
(54) Tomasi, J.; Persico, M. *Chem. Rev.* **1994**, *94*, 2027.
(55) Laws, W. R.; Brand, L. *J. Phys. Chem.* **1979**, *83*, 795.
(56) Marcus, R. A. *J. Phys. Chem.* **1989**, *93*, 3078.
(57) Koutek, B. *Collect. Czech. Chem. Commun.* **1978**, *43*, 2368.
(58) Mataga, N.; Kubota, T. *Molecular Interactions and Electronic Spectra*; Mercel Dekker: New York, 1970.
(59) Assuming the conditions leading to eq 3.1, eq 5.1 is exact, which can be seen from

$$\varphi_{LE} = k_{LE}^{rad}\int_0^\infty [LE(t)]\,dt/[LE(0)] = k_{LE}^{rad}\int_0^\infty I(t)\,dt/I(0) = k_{LE}^{rad}\langle\tau_{LE}\rangle$$

(60) Van der Auweraer, M.; Grabowski, Z. R.; Rettig, W. *J. Phys. Chem.* **1991**, *95*, 2083.
(61) Rettig, W.; Bliss, B.; Dirnberger, K. *Chem. Phys. Lett.* **1999**, *305*, 8.
(62) Schuddenboom, W.; Jonker, S. A.; Warman, J. M.; Leinhos, U.; Kühnle, W.; Zachariasse, K. A. *J. Phys. Chem.* **1992**, *96*, 10809.
(63) Druzhinin, S. I.; Demeter, A.; Galievsky, V. A.; Yoshihara, T.; Zachariasse, K. A. *J. Phys. Chem. A* **2003**, *107*, 8075.
(64) Il'ichev, Y. V.; Kühnle, W.; Zachariasse, K. A. *J. Phys. Chem. A* **1998**, *102*, 5670.
(65) Birks, J. B. *Photophysics of Aromatic Molecules*; Wiley: London, 1970.
(66) Lewis, J. E.; Maroncelli, M. *Chem. Phys. Lett.* **1998**, *282*, 197.
(67) Okada, T.; Uesugi, M.; Köhler, G.; Rechthaler, K.; Rotkiewicz, K.; Rettig, W.; Grabner, G. *Chem. Phys.* **1999**, *241*, 327.
(68) Dorairaj, S.; Kim, H. J. *J. Phys. Chem. A* **2002**, *106*, 2322.
(69) van der Zwan, G.; Hynes, J. T. *J. Phys. Chem.* **1985**, *89*, 4181.
(70) Böttcher, C. J. F.; van Belle, O. C.; Bordewijk, P.; Rip, A. *Vol. 1: Theory of Electric Polarization: Dielectrics in Static Fields*; Elsevier: Amsterdam, 1973; Vol. I.
(71) W. Song and M. Maroncelli, unpublished results of AM1/CI calculations using the COSMO solvation method.
(72) Gorse, A.-D.; Pesquer, M. *J. Phys. Chem.* **1995**, *99*, 4039.
(73) Cave, R.; Newton, M. *Chem. Phys. Lett.* **1996**, *249*, 15.
(74) Because the L_b and L_a mixing is small near the LE and CT geometries in the gas phase, these properties of the diabatic states are simply the properties of the adiabatic S_1 and S_2 to which proper association has been made on the basis of transition moment directions.
(75) Bondi, A. *J. Phys. Chem.* **1964**, *68*, 441.
(76) This relationship is based on correlating the experimental polarizabilities of 49 solutes with estimated van der Waals volumes. Similar cavity radii are obtained using linear correlations established by Brinck et al.[94]

(77) Press, W.; Flannery, B.; Teukolsky, S.; Vetterling, W. *Numerical Recipies—The Art of Scientific Computing*; Cambridge University Press: Cambridge, 1986.

(78) Bevington, P. R. *Data Reduction and Error Analysis for the Physical Sciences*; McGraw-Hill: New York, 1969.

(79) To compare the peak frequencies derived from the fits to the geometry optimized energies from the semiempirical calculations, we have approximately accounted for the difference between 0-0 and vertical transition energies by shifting the calculated values in the manner $U_a^{LE} \rightarrow U_a^{LE} + \Delta$, $U_b^{LE} \rightarrow U_b^{LE} - \Delta$, and $U_a^{CT} \rightarrow U_a^{CT} - \Delta$ with an estimated solute-independent value of $\Delta = 3000$ cm^{-1}.

(80) For example, because the frequencies and relative intensities are differently sensitive to electronic and nuclear solvent polarizability, one might suppose that a frequency-resolved cavity model of the sort proposed by Newton and co-workers[95] might work better than a single-cavity approach. However, we find that such an approach worsens the agreement between the model and experiment.

(81) This idea is far from new. See for example, the discussion in refs 1, 60, and 96.

(82) Koti, A. S. R.; Krishna, M. M. G.; Periasamy, N. *J. Phys. Chem. A* **2001**, *105*, 1767.

(83) Koti, A. S. R.; Periasamy, N. *Res. Chem. Intermed.* **2002**, *28*, 831.

(84) Chapman, C. F.; Fee, R. S.; Maroncelli, M. *J. Phys. Chem.* **1995**, *99*, 4811.

(85) Su, S.-G.; Simon, J. D. *J. Phys. Chem.* **1989**, *93*, 753.

(86) We note that similar quantities were defined more rigorously in theoretical work of Marcus and co-workers[35] and previously applied to DMABN by Su and Simon.[28]

(87) Hynes, J. T. The Theory of Reactions in Solution. In *The Theory of Chemical Reactions*; Baer, M., Csizmadia, I. G., Eds.; CRC Press: Boca Raton, 1985; p 171.

(88) Fleming, G. R.; Hanggi, P. *Activated Barrier Crossing*; World Scientific: Singapore, 1993.

(89) This estimate is based on semiempirical (AM1/CI) calculations of the LE ($\theta = 0$) S_0 and S_1 wells. In the case of P4C one can identify a normal mode which is purely of the twisting character usually assumed for the reaction coordinate. In the higher members of the P*n*C series twisting of the amino group as a whole is mixed with internal torsional motions of the group and no single normal mode is clearly identified with the reaction coordinate. Nevertheless, the modes that twist the amino group in the requisite manner all tend to fall in the region between 50 and 150 cm^{-1}, and the value of 75 cm^{-1} is representative.

(90) Rettig, W.; Fritz, R.; Braun, D. *J. Phys. Chem. A* **1997**, *101*, 6830.

(91) Shaik, S. S.; Schlegel, H.; Wolfe, S. *Theoretical Aspects of Physical Organic Chemistry*; Wiley: New York, 1992.

(92) These calculations use the COSMO solvation model[52] with a solvent radius of 2.6 Å. For ease of calculation the geometry of the solute was maintained at the optimized geometry of the LE minimum and only the twist angle θ varied.

(93) Kwok, W. M.; George, M. W.; Grills, D. C.; Ma, C.; Matousek, P.; Parker, A. W.; Phillips, D.; Toner, W. T.; Towrie, M. *Angew. Chem., Int. Ed. Engl.* **2003**, *42*, 1826.

(94) Brinck, T.; Murray, J. S.; Politzer, P. *J. Chem. Phys.* **1993**, *98*, 4305.

(95) Basilevsky, M. V.; Rostov, I. V.; Newton, M. D. *Chem. Phys.* **1998**, *232*, 189.

(96) Rettig, W.; Rotkiewicz, K.; Rubaszewska, W. *Spectrochim. Acta* **1984**, *40A*, 241.